Hindawi
Mathematical Problems in Engineering
Volume 2019, Article ID 7182539, 22 pages
https://doi.org/10.1155/2019/7182539

Research Article

A Parameter Adaptive MOMEDA Method Based on Grasshopper Optimization Algorithm to Extract Fault Features

ChengJiang Zhou[1,2] **Jun Ma**[1,2] **Jiande Wu**[1,2] **and Zezhong Feng**[1,2]

[1]*Faculty of Information Engineering and Automation, Kunming University of Science and Technology, Kunming 650500, China*
[2]*Engineering Research Center for Mineral Pipeline Transportation of Yunnan Province, Kunming 650500, China*

Correspondence should be addressed to Jun Ma; majun_km@foxmail.com

Received 5 September 2018; Revised 8 December 2018; Accepted 13 January 2019; Published 5 March 2019

Academic Editor: Changzhi Wu

Copyright © 2019 ChengJiang Zhou et al. This is an open access article distributed under the Creative Commons Attribution License, which permits unrestricted use, distribution, and reproduction in any medium, provided the original work is properly cited.

The nonstationary components and noises contained in the bearing vibration signal make it particularly difficult to extract fault features, and minimum entropy deconvolution (MED), maximum correlated kurtosis deconvolution (MCKD), and fast spectral kurtosis (FSK) cannot achieve satisfactory results. However, the filter size and period range of multipoint optimal minimum entropy deconvolution adjusted (MOMEDA) need to be set in advance, so it is difficult to achieve satisfactory filtering results. Aiming at these problems, a parameter adaptive MOMEDA feature extraction method based on grasshopper optimization algorithm (GOA) is proposed. Firstly, the multipoint kurtosis (MKurt) of MOMEDA filtered signal is used as the optimization objective, and the optimal filter size and periodic initial value which matched with the vibration signal can be determined adaptively through multiple iterations of GOA. Secondly, the periodic impact contained in the vibration signal is extracted by the optimized MOMEDA, and the fault features in the impact signal are extracted by Hilbert envelope demodulation. Finally, the simulation signal and bearing signal are processed by the proposed approach. The results show that the introduction of GOA not only solves the problem of parameter selection in MOMEDA, but also achieves better performance compared with other optimization methods. Meanwhile, the feasibility and superiority of the approach are fully proved by comparing it with the three methods MED, MCKD, and FSK after parameter optimization. Therefore, this approach provides a novel way and solution for fault diagnosis of the rolling bearing, gear, and shaft.

1. Introduction

The bearing is an important rotating part widely used in manufacturing, transportation, aerospace, and other fields, and one of the most vulnerable rotating components. Bearing failure may cause catastrophic damage to the rotating machinery and lead to serious loss of life and property. Therefore, bearing health monitoring and fault diagnosis are particularly important [1]. At present, the time-frequency analysis technology is the most popular feature extraction method. However, the bearing vibration signal contains complex background noise and interference components, and satisfactory feature extraction results cannot be obtained by using the traditional time-frequency analysis methods [2]. Therefore, it is of great significance to explore the simple and effective feature extraction methods.

The fault impact and vibration source can be extracted from the vibration signal by Hilbert envelope demodulation [3]. However, this method is only applicable to the single AM-FM signal. Therefore, signal preprocessing is required before demodulation. Signal decomposition and mode selection are the most commonly used preprocessing methods. The empirical mode decomposition (EMD) [4] is the most classical method. In order to prevent mode mixing caused by the discontinuous signal in the screening process, ensemble empirical mode decomposition (EEMD) [5], complete ensemble empirical mode decomposition adaptive noise (CEEMDAN) [6], and other methods were proposed. Zhou et al. [7] first decomposed the bearing signal into several modes by EEMD, then extracted the weighted permutation entropy (PE) of the previous modes, and diagnosed the bearing faults through SVM ensemble classifier. Lv et al. [8] decomposed the bearing

signal by CEEMDAN and calculated the improved multivariate multiscale sample entropy of the effective modes, and the method realizes the bearing early fault diagnosis. Inspired by EMD, Smith et al. proposed local mean decomposition (LMD) [9]. In order to improve its mode mixing problem, a variety of improved methods have been proposed, such as ensemble local mean decomposition (ELMD) [10], complete ensemble local mean decomposition (CELMD) [11], etc. Zhang et al. [12] proposed a weak fault diagnosis method based on mask signal and LMD, which can not only suppress the modal mixing of LMD but also effectively extract the fault features. Wang et al. [13] decomposed the bearing signal by ELMD and then selected the effective product functions (PF) according to kurtosis and finally extracted the fault pulse information by using fast spectral kurtosis (FSK). Recently, variational mode decomposition (VMD) [14], empirical wavelet transform (EWT) [15], and other methods have been used for signal decomposition. Wang et al. [16] proposed an improved VMD based on PE and white noise, which can adaptively select the mode number of VMD and is insensitive to noise. Zhang et al. [17] proposed an adaptive VMD based on grasshopper optimization algorithm (GOA), which can adaptively determine the parameters of VMD according to the signal characteristics, and the decomposition performance of the algorithm is improved. Wang et al. [18] proposed the sparsity guided EWT, which can automatically establish the Fourier segments required by empirical wavelet transform. Luo et al. [19] proposed the autoregressive EWT, which detects the boundaries of the autoregressive power spectrum by Burg algorithm. This method avoids the error boundary caused by white noise and nonstationary signal. Through these methods, the signal is decomposed into many subsignals in different frequency bands. Then, some indicators are often used to determine sensitive modes, including correlation coefficient, kurtosis, energy, and entropy. Furthermore, FSK [20], cyclostationary analysis (CA) [21], stochastic resonance (SR) [22], and other signal processing methods have also received increasing attention.

The deconvolution method is another effective signal processing method, which can extract the impact components contained in the vibration signal. Minimum entropy deconvolution (MED) and maximum correlation kurtosis deconvolution (MCKD) are the most popular deconvolution methods. Endo et al. used MED to diagnose the fault of rotating machinery for the first time [23]. Li et al. [24] determined the filter size of MED by constructing the power spectral kurtosis index and then extracted the impact components in the filtered signal by time-delay feedback mono-stable stochastic resonance. Abboud et al. [25] enhanced the impact component of the signal through MED, then constructed the optimal frequency band by FSK, and finally extracted fault features by Hilbert envelope demodulation. Although mechanical faults can be detected by MED, the MED filter is not necessarily the optimal filter. In addition, the periodic impact signals contained in the vibration signal cannot be efficiently extracted by MED. Mcdonald et al. [26] proposed MCKD, which can extract a series of fault impacts from the vibration signal. Wan et al. [27] calculated the period of MCKD according to the estimated characteristic frequency and then extracted the early fault features contained in the filtered signal by FSK. The period and filter size of MCKD need to be set in advance, so the method lacks adaptability. In 2017, McDonald et al. [28] proposed the multipoint optimal minimum entropy deconvolution adjusted (MOMEDA). The method does not require the iterative solution in the filtering process, and it can extract the periodic fault impact according to the multipoint kurtosis (MKurt) in the period range [29]. Wang et al. [30] successfully extracted the multiple impact components from the simulation signal and gearbox vibration signal by MOMEDA. Zhu et al. [31] extracted the impact components from the bearing signal by MOMEDA and then extracted the fault features by Teager energy operator (TEO). Wang et al. [32] analyzed the variable speed signal by MOMEDA and resampling order analysis technology and achieved good results. Since the early fault features of the gearbox are often submerged by strong noise, Wang et al. [33] first used MED to suppress the noise and then extracted the composite fault features from the denoised signal by MOMEDA. Cai et al. [34] first used the ELMD and correlation coefficients to obtain the sensitive modes, and they used the combined product function method (CPF) to recombine the PF with the same period. Finally, periodic fault impacts in the combined signal were extracted by MOMEDA. Thus, the MOMEDA has been increasingly used in periodic impact extraction and fault diagnosis.

In the deconvolution algorithm, a measure of a signal (also known as a norm) is first defined, and then a filter is constructed to maximize the norm of the filtered signal [28]. The norms of MED, MCKD, and MOMEDA are kurtosis, correlation kurtosis (CK), and multipoint kurtosis (MKurt), respectively. In the methods, MED and MCKD, the filter size and the number of iterations affect the norm of the filtered signal. In addition, the period is the main factor influencing the filtering effect of the MCKD. Therefore, the parameter optimization of deconvolution algorithms is particularly important, and the existing methods are mostly based on kurtosis. Cheng et al. [35] optimized the filter parameters of MED by particle swarm optimization (PSO) and then successfully extracted fault features by optimized MED. Instance et al. [36] optimized the filter size and the number of iterations of MED by shuffled frog leaping algorithm (SFLA), and the method avoids the subjectivity of artificially selected parameters. Miao et al. [37] estimated the period of MCKD by calculating the autocorrelation of envelope signals and improved the resampling process of MCKD. The above methods improve the filtering performance of MED and MCKD and provide the new idea and way for the parameter optimization problem of MOMEDA. The filter size and periodic initial value seriously affect the filtering results of MOMEDA. Meanwhile, the effects of these two parameters on the filtering results are nonlinear and complicated, and the satisfactory filtering results cannot be obtained by selecting random parameters. Therefore, the parameter optimization of MOMEDA is of great significance. Nowadays, many novel optimization methods are attracting attention, such as bat algorithm (BA), flower pollination algorithm (FPA), and cuckoo search algorithm (CS), etc. Saremi et al. [38] proposed the GOA in 2017 and compared it with a variety

of optimization algorithms. The results show that GOA has outstanding advantages in optimizing the unimodal function, multimodal function, and compound function. Zhang et al. [17] optimized the mode number and penalty factor of VMD by GOA, which not only improved the performance of VMD but also improved the effects of feature extraction. Barman et al. [39] optimized the kernel function and penalty factor of support vector machine (SVM) by GOA and then used the model to predict the power load in the local climate.

To solve the parameter selection problem of MOMEDA, a parameter adaptive MOMEDA method based on GOA is proposed, which combines the advantages of GOA and MOMEDA effectively. Firstly, the algorithm parameters are initialized according to the signal characteristics. Then, we optimize MOMEDA parameters by GOA algorithm. In each iteration, the impact component contained in the mixed signal is extracted by MOMEDA, and the opposite of the MKurt is served as the objective function to optimize the filter parameters. Finally, the optimized MOMEDA is used to extract the impact component from the signals, and the fault feature is extracted through Hilbert envelope demodulation. In order to prove the validity of the proposed approach, the method is used to analyze the simulation signal, Case Western Reserve University (CWRU) bearing dataset [40], and National Aeronautics and Space Administration (NASA) bearing dataset [41]. To highlight the advantages of GOA, the algorithm is compared with PSO, SFLA, and gray wolf optimization algorithm (GWO) [42], and then the proposed approach is compared with the MOMEDA methods with fixed parameters. Finally, the proposed approach is compared with the three methods, MED, MCKD, FSK after parameter optimization. The structure of the paper is shown in Figure 1(b).

The main contents of the paper are as follows. Theories of MOMEDA and GOA are introduced briefly in Section 2. The process of optimizing MOMEDA filter parameters is introduced in Section 3. The validity of the proposed approach is verified by simulation signal in Section 4. In Section 5, the validity and reliability of the approach are validated by CWRU dataset and NASA dataset. In Section 6, the experimental process and preliminary conclusions are discussed. The conclusions of the experiment are summarized in Section 7.

2. A Brief Review of the Diagnostic Techniques

2.1. MOMEDA. The response signal can be expressed as follows [33, 34, 43]:

$$y(n) = h(n) * x(n) + e(n), \tag{1}$$

where $y(n)$ is the vibration signal, $x(n)$ is the impact component, $h(n)$ is the system frequency response function, and $e(n)$ is the background noise. In order to reconstruct the impact component, the deconvolution process is as follows:

$$x(n) = f(n) * y(n) = \sum_{l=1}^{L} f_l y_{k+L-1}. \tag{2}$$

In (2), $k = 1, 2, \cdots, N - L$, where N represents the signal length and L represents the filter size. In view of the characteristics of the periodic impact signal, the multipoint D-norm is introduced in this method, as shown below.

$$Multi\ D-Norm = MDN\left(\vec{y}, \vec{t}\right) = \frac{1}{\left\|\vec{t}\right\|} \frac{\vec{t}^{T}\vec{y}}{\left\|\vec{y}\right\|}. \tag{3}$$

$$MOMEDA = \max_{\vec{f}} MDN\left(\vec{y}, \vec{t}\right) = \max_{\vec{f}} \frac{\vec{t}^{T}\vec{y}}{\left\|\vec{y}\right\|}, \tag{4}$$

where $\vec{t}$ represents a constant vector and it is used to describe the position and weight of the target impact. The optimal filter can be obtained by solving the maximum of multipoint D-norm, and the deconvolution process also obtains the optimal solution at this time. In order to calculate the extreme value of (4), we first calculate the derivative of the filter coefficients $\vec{f} = (f_1, f_2, \cdots, f_L)$.

$$\begin{aligned}\frac{d}{d\vec{f}}\left(\frac{\vec{t}^{T}\vec{y}}{\left\|\vec{y}\right\|}\right) = \frac{d}{d\vec{f}}\frac{t_1 y_1}{\left\|\vec{y}\right\|} + \frac{d}{d\vec{f}}\frac{t_2 y_2}{\left\|\vec{y}\right\|} + \cdots \\ + \frac{d}{d\vec{f}}\frac{t_{N-L} y_{N-L}}{\left\|\vec{y}\right\|}.\end{aligned} \tag{5}$$

$$\frac{d}{d\vec{f}}\frac{t_k y_k}{\left\|\vec{y}\right\|} = \left\|\vec{y}\right\|^{-1} t_k \vec{M}_k - \left\|\vec{y}\right\|^{-3} t_k y_k X_0 \vec{y}. \tag{6}$$

$$\vec{M}_k = \left[x_{x+L-1}, x_{x+L-2}, \cdots, x_k\right]^{T}. \tag{7}$$

Therefore, (5) can be transformed into the following form.

$$\begin{aligned}&\frac{d}{d\vec{f}}\left(\frac{\vec{t}^{T}\vec{y}}{\left\|\vec{y}\right\|}\right) \\ &= \left\|\vec{y}\right\|^{-1}\left(t_1\vec{M}_1 + t_2\vec{M}_2 + \cdots t_{N-L}\vec{M}_{N-L}\right) \\ &\quad - \left\|\vec{y}\right\|^{-3}\vec{t}^{T}\vec{y}X_0\vec{y}.\end{aligned} \tag{8}$$

The equation $t_1\vec{M}_1 + t_2\vec{M}_2 + \cdots t_{N-L}\vec{M}_{N-L} = X_0\vec{t}$ is used to simplify the formula above, and (5) is equivalent to the following formula.

$$\left\|\vec{y}\right\|^{-1} X_0\vec{t} - \left\|\vec{y}\right\|^{-3}\vec{t}^{T}\vec{y}X_0\vec{y} = \vec{0}. \tag{9}$$

Then, the equation $(\vec{t}^{T}\vec{y}/\|\vec{y}\|^2)X_0\vec{y} = X_0\vec{t}$ can be obtained. Since $\vec{y} = X_0{}^{T}\vec{f}$, assuming $(X_0X_0{}^{T})^{-1}$ exists, the following formula can be obtained.

$$\frac{\vec{t}^{T}\vec{y}}{\left\|\vec{y}\right\|^2}\vec{f} = \left(X_0X_0{}^{T}\right)^{-1}X_0\vec{t}. \tag{10}$$

The special solution of (10) is a set of optimal filters, and the optimal filters can be expressed as follows.

Initialize the swarm $X_i(1, 2, \cdots, n)$
Initialize maximum number of iterations M, $c_{\max}$ *and* $c_{\min}$
Calculate the fitness of each search agent
T=the best search agent
while *(m<Max number of iterations M)*
  Update c using Eq. (18)
  for *each search agent*
    Normalize the distances between grasshoppers in [1,4]
    Update the position of the current search agent by Eq . (17)
    Bring the current search agent back if it goes outside boundaries
  end for
  Update T, if there is a better solution
  m=m+1
end while
Return T

(a) The implementation process of GOA

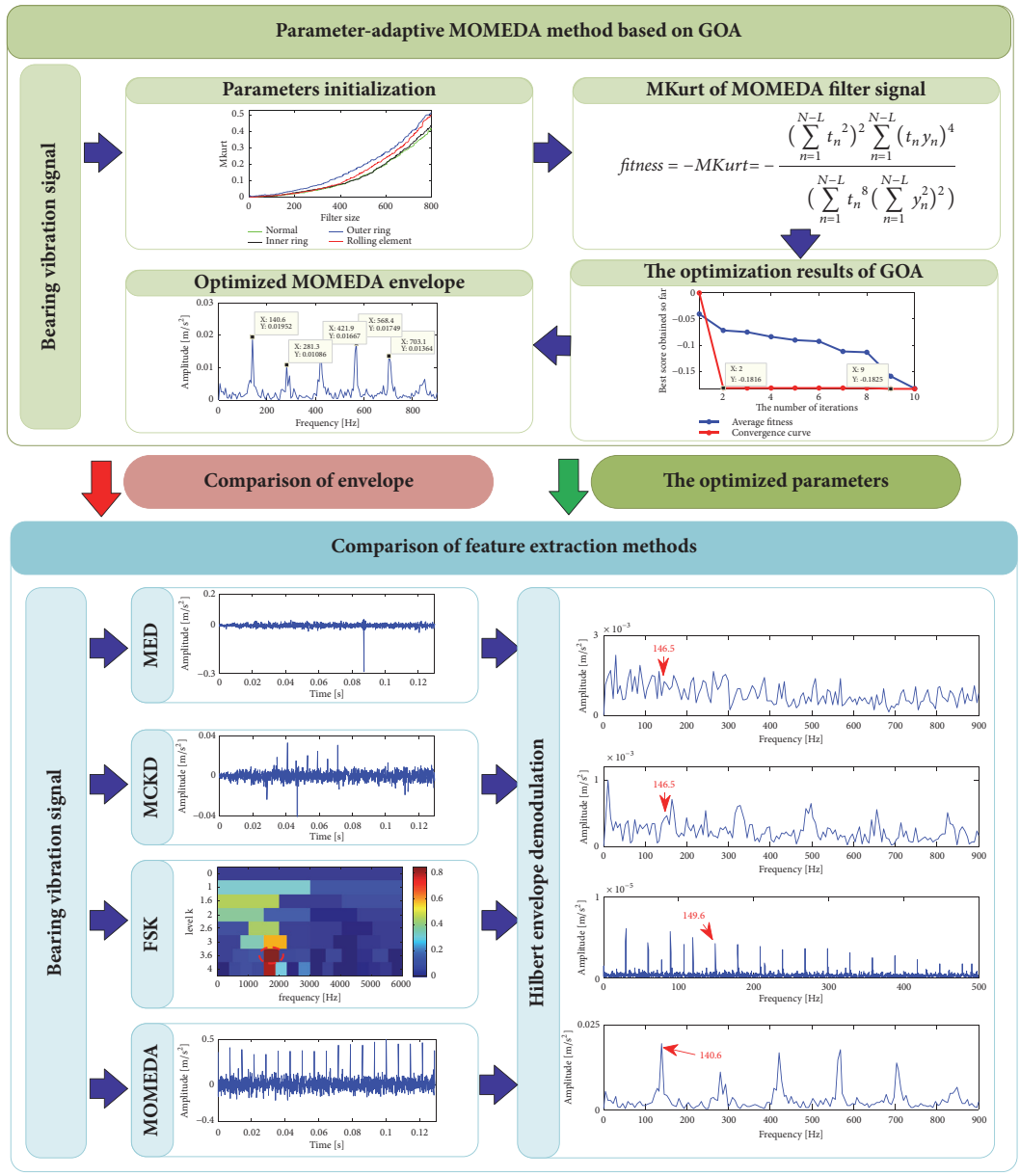

(b) Parameter optimization process of MOMEDA

Figure 1: Parameter optimization process and the structure of the paper.

$$\overrightarrow{f} = \left(X_0 X_0^{\,T}\right)^{-1} X_0 \overrightarrow{t}. \tag{11}$$

$$X_0 = \begin{bmatrix} x_L & x_{L+1} & x_{L+2} & \cdots & x_N \\ x_{L-1} & x_L & x_{L+1} & \cdots & x_{N-1} \\ x_{L-2} & x_{L-1} & x_L & \cdots & x_{N-2} \\ \vdots & \vdots & \vdots & \ddots & \vdots \\ x_1 & x_2 & x_3 & \cdots & x_{N-L+1} \end{bmatrix}_{L \text{ by } N-L+1}. \tag{12}$$

Then, the original impact signal can be reconstructed by the formula $\overrightarrow{y} = X_0^{\,T} \overrightarrow{f}$.

2.2. GOA. GOA is a new bionic algorithm, which simulates the foraging behavior of the grasshoppers [38]. The behavior of grasshoppers has the following characteristics: the nymphs move slowly and the step size of movement is small, while the adults move fast in a wide range of parameter space. Therefore, the search mechanism of the GOA algorithm consists of two tendencies: exploration and exploitation. The algorithm optimizes the objective function by judging the repulsion region, comfort zone, and attraction region formed between the grasshoppers. GOA has the advantages of few parameters and high convergence accuracy. The mathematical model of GOA [38] is as follows.

(1) The Initialization of the Population. The grasshoppers random behavior can be represented by the following model.

$$X_i = S_i + G_i + A_i, \tag{13}$$

$$\begin{aligned} S_i &= \sum_{j=1, j\neq i}^{N} s\left(d_{ij}\right) \widehat{d_{ij}} \\ G_i &= -g\widehat{e_g} \\ A_i &= u\widehat{e_w}, \end{aligned} \tag{14}$$

where X_i represents the location of the i-th grasshopper, S_i refers to the social interaction, G_i represents the gravity force of the i-th grasshopper, and A_i represents the wind advection. In (14), N represents the number of grasshoppers, d_{ij} represents the distance between the i-th and the j-th individual, and $d_{ij} = |x_j - x_i|$, $\widehat{d_{ij}} = (x_j - x_i)/d_{ij}$ represents a unit vector. The s function is shown in (15), which represents the social forces. g represents the gravitational constant, and $\widehat{e_g}$ represents a unit vector pointing to the earth. u is a constant drift, and $\widehat{e_w}$ represents a unit vector towards the wind direction.

$$s(r) = fe^{-r/l} - e^{-r}, \tag{15}$$

where f represents the intensity of attraction and l represents the attractive length scale.

(2) Location Update. Substituting S_i, G_i, and A_i in (13), the specific position of the i-th grasshopper is as follows.

$$X_i = \sum_{j=1, j\neq i}^{N} s\left(\left|x_j - x_i\right|\right) \frac{x_j - x_i}{d_{ij}} - g\widehat{e_g} + u\widehat{e_w}. \tag{16}$$

Equation (16) shows that the grasshoppers move quickly to the comfort zone, at which point the swarm has not found a specified point. Therefore, the model needs to be improved before solving optimization problems. Actually, the model is considered in free space, and the gravity need not be considered (no G_i component). At the same time, we assume that the wind direction is the same as the target direction ($\widehat{T_d}$). An improved version of (16) is as follows:

$$\begin{aligned} X_i^d = c\left(\sum_{j=1, j\neq i}^{N} c\frac{ub_d - lb_d}{2} s\left(\left|x_j^d - x_i^d\right|\right) \frac{x_j - x_i}{d_{ij}}\right) \\ + \widehat{T_d}, \end{aligned} \tag{17}$$

where ub_d and lb_d are the upper and lower boundaries of the D-dimensional search space, respectively. $\widehat{T_d}$ represents the optimal solution found so far in the target direction. The outer c adjusts the exploration and exploitation of the swarm near the target. Inner c reduces the interaction between grasshoppers as the iteration number increases.

(3) Balance of Search Ability. The parameter c is used to balance the exploration and exploitation of the swarm, which decreases linearly with the increase of iteration. This mechanism reduces the comfort zone and thus enhances the exploitation ability.

$$c = c_{\max} - m\frac{c_{\max} - c_{\min}}{M}, \tag{18}$$

where $c_{\max}$ and $c_{\min}$ are the upper and lower boundaries of c, respectively, and they take 1 and 0.00004 in this paper. m represents the current iteration, and M represents the maximum number of iterations.

3. Parameter Adaptive MOMEDA Method Based on GOA

Kurtosis can characterize the distribution density of the impact signal, and it has been widely used in signal processing. MKurt is based on kurtosis; it not only inherits the characteristics of the kurtosis but also extends its definition to multiple pulses at controlled locations [28, 33]. Therefore, MKurt can not only provide location information of fault, but also indicate the energy and period of the fault signal [29]. Meanwhile, a larger MKurt characterizes a larger proportion of the periodic impacts [33].

$$MKurt = \frac{\left(\sum_{n=1}^{N-L} t_n^{\,2}\right)^2 \sum_{n=1}^{N-L} \left(t_n y_n\right)^4}{\left(\sum_{n=1}^{N-L} t_n^{\,8} \left(\sum_{n=1}^{N-L} y_n^2\right)^2\right)}. \tag{19}$$

So we expect to get the maximum of MKurt and the parameters of MOMEDA when the maximum is reached in this paper. Since the intention of GOA is to search for the minimum of the objective function [17], the opposite of MKurt is used as the objective function in this paper.

$$\begin{aligned} fitness = \min_{\gamma=\{L, T_i\}} \{-MKurt\} \\ L \in [1, 500], \; T_i \in [50, 150], \end{aligned} \tag{20}$$

where *fitness* is the objective function and $\gamma = (L, T_i)$ is a set of parameters that need to be optimized. L is a positive integer within range $L \in [1, 500]$, and T_i takes a value in range $T_i \in [50, 150]$. The steps of the approach are as follows:

(1) Input the signal $x(t)$, and initialize the ranges of the MOMEDA parameters. Meanwhile, initialize the GOA parameters and grasshoppers swarm.

(2) Extract the periodic impact signal by using MOMEDA, and calculate the fitness of the impact signal. Save the best fitness and corresponding position $\widehat{T_d}$ for each iteration of GOA.

(3) If the current iteration m is less than the maximum M, the decreasing coefficient c is updated by (18).

(4) For each swarm, normalize the distances between individuals in [1, 4], and update the location of the search agent by (17).

(5) If there is a better solution, update the best fitness and corresponding position $\widehat{T_d}$. Then, determine if the stop criterion is reached ($m \geq M$). If yes, the iteration is terminated. Else, let $m = m + 1$, and the iteration will be continued.

(6) Obtain the best fitness and the corresponding parameters of MOMEDA.

(7) Extract the periodic impact signal by using MOMEDA with the optimized parameters.

(8) Extract fault features from impact signal by using Hilbert envelope demodulation.

4. Simulations and Comparisons

To verify the feasibility of the approach, we analyzed the bearing simulation signal [44] by using the proposed method. Meanwhile, all the experiments were completed by using MATLAB R2014a under the environment of Intel(R) Core(TM) i5-5200U CPU @ 2.20GHz 2.19GHz, 8GRAM.

$$x(t) = y_0 e^{-2\pi f_n \xi t} * \sin\left(2\pi f_n * \sqrt{1-\xi^2}t\right), \quad (21)$$

where the natural frequency $f_n = 3000Hz$, damping coefficient $\xi = 0.1$, shift constant $y_0 = 2.5$, impact period $T = 0.00625s$ (characteristic frequency theoretical value $f_{chthe} = 160Hz$), data length $N = 4096$, and sampling frequency $f_s = 12KHz$. Moreover, the 5 dB noise is mixed into the original signal.

The waveforms of the simulation signal and noisy signals are given in Figure 2. In Figure 2(b), the frequency $f_{chthe} = 160Hz$ and its harmonics are especially obvious. In Figures 2(c) and 2(d), the characteristic frequency of the noisy signal and harmonics are submerged by noise. Although the noisy signal is similar to the actual bearing fault signal, the waveforms of the noisy signal are more complex [44].

Then, we analyze the noisy signal by the proposed approach. Here, the search agents $S_{An} = 100$, the maximum number of iterations $M = 10$, and the ranges of filter size and the periodic initial value are $L \in [1, 500]$ and $T_i \in [50, 150]$, respectively. As shown in Figure 3, along with the increasing of iterations, the grasshopper swarms tend to converge towards the best locations, and the convergent curve gradually converges to the minimum. When the number of iterations $m = 9$, the MKurt ($MKurt = 0.31328$) reaches the maximum, and the optimal parameters $\gamma = (L, T_i) = (386, 75.00464)$ of MOMEDA are obtained. Then, the impact signal in the noisy signal is extracted by the optimized MOMEDA, and the envelope of the impact component is given in Figure 4. The actual value of the characteristic frequency $f_{ch} = 161.1$Hz is approximate to $f_{chthe} = 160Hz$, and its harmonics are particularly obvious. Therefore, the proposed approach is feasible in extracting the features from the noisy signal.

In order to explore the effect of nonoptimal parameters on the results, we compared four sets of MOMEDA methods with fixed parameters. As shown in Figures 5(a) and 5(b), when the filter size L of MOMEDA is the optimal value $L = 386$ obtained by GOA and periodic initial value $T_i = 50$, the frequency 240.2Hz and its harmonics can be observed clearly. Meanwhile, when $T_i = 90$, the frequency 134.8Hz and its harmonics are obvious. However, the frequency 240.2 Hz is far greater than the theoretical value of the characteristic frequency ($f_{chthe} = 160Hz$), and the frequency 134.8 Hz is far less than the theoretical value. Therefore, the improper selection of periodic initial value could lead to incorrect diagnostic results. As shown in Figures 5(c) and 5(d), when T_i of MOMEDA is set to the optimal value $T_i = 75.00464$, the frequency 158.2 Hz and its harmonics can be observed clearly, and these frequencies are approximate to $f_{chthe} = 160Hz$ and its harmonics. Meanwhile, the spectral peaks of the envelope spectrum are more obvious when $L = 900$.

Figure 5 shows that the selection of filter size and periodic initial value has a great impact on the feature extraction results. Therefore, it is important to choose an effective optimization method. Next, we discuss the optimization performance of PSO, SFLA, GWO, and GOA. For comparison purposes, the maximum number of iterations and population numbers of all algorithms are set to 50 and 20, and the other parameters are the default values. The -6db noise is mixed into the original signal, and the waveforms of the noisy signal are shown in Figures 2(e) and 2(f).

As shown in Figure 6 and Table 1, the optimal fitness (-0.075004) obtained by PSO is greater than that obtained by GOA when the number of iterations is 29, and the results show that the optimization precision of PSO is not high. Moreover, the convergence speed of PSO is slow and the algorithm is time-consuming. The convergence speed of the SFLA is fast, and the iterations take little time. However, the optimal fitness (-0.0746) obtained by SFLA is greater than that of other algorithms, which indicates that the optimization precision of the SFLA is lower than that of other methods. The GWO has high convergence accuracy, but its convergence speed is very slow and the optimal fitness is obtained through 49 iterations. Compared with the above methods, the convergence speed of GOA is very fast. The optimal parameters are obtained when the number of iterations is 25. Moreover, the optimal fitness obtained by GOA is minimal. It can be concluded that GOA is not only simple in calculation, but also high in convergent speed and accuracy. The GOA has outstanding advantages compared

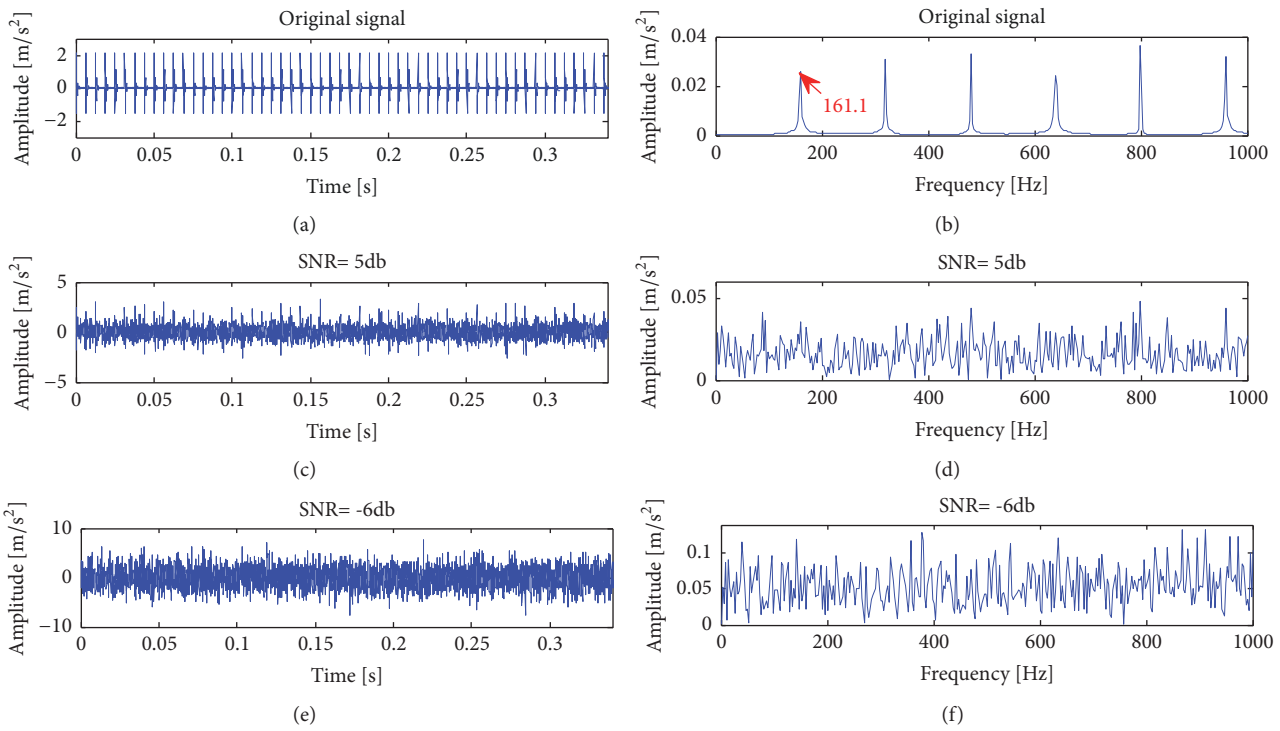

Figure 2: Noisy signals and their frequency domain.

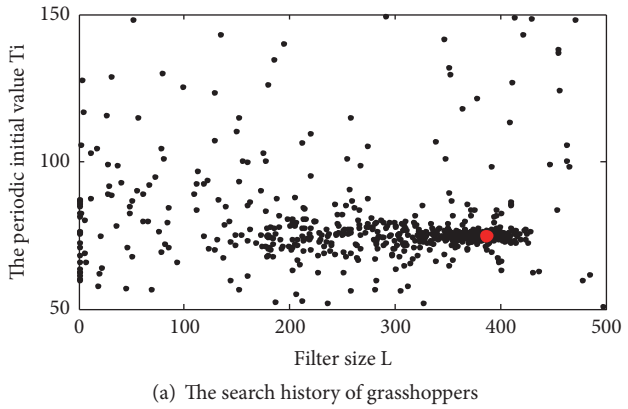

(a) The search history of grasshoppers

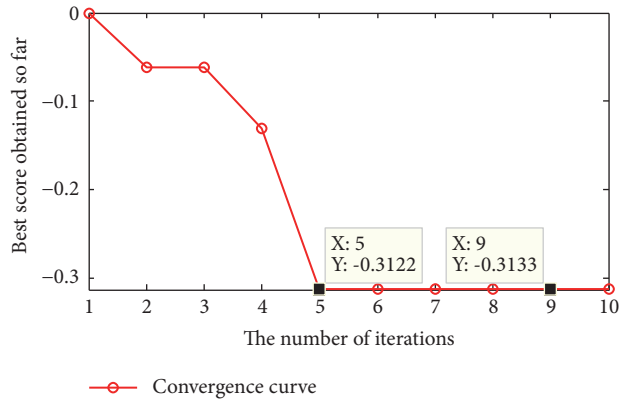

(b) Convergence curve of GOA

Figure 3: Optimization results of MOMEDA.

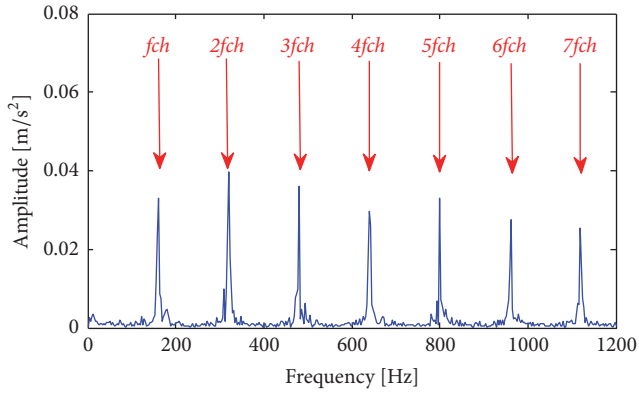

Figure 4: The envelope of the impact signal.

with other optimization algorithms, so we optimized the parameters of the MOMEDA by using GOA in this paper.

To highlight the advantage of the approach, the method is compared with the methods with the optimal parameters, such as MED, MCKD, and FSK. Since the norms of MED, MCKD, and MOMEDA are based on kurtosis, the optimal filter size $L = 386$ obtained by GOA is used as the filter size of MED and MCKD, and the optimal periodic initial value $T_i = 75.00464$ is taken as the period of MCKD. The number of iterations of MED and MCKD is both set to 30. Compared with the method in the literature [27], the method has good adaptability. According to the characteristic of the noisy signal, the decomposition level of FSK is 4. In

Table 1: The optimization results of algorithms.

Index	PSO	SFLA	GWO	GOA
Fitness	-0.075004	-0.07468	-0.07616	-0.076541
Time (s)	356.8335	294.9474	369.3333	321.8644
Convergence	29	27	49	25
Best L	500	478	494	494
Best T_i	75.0050	72.2673	74.7739	74.99123

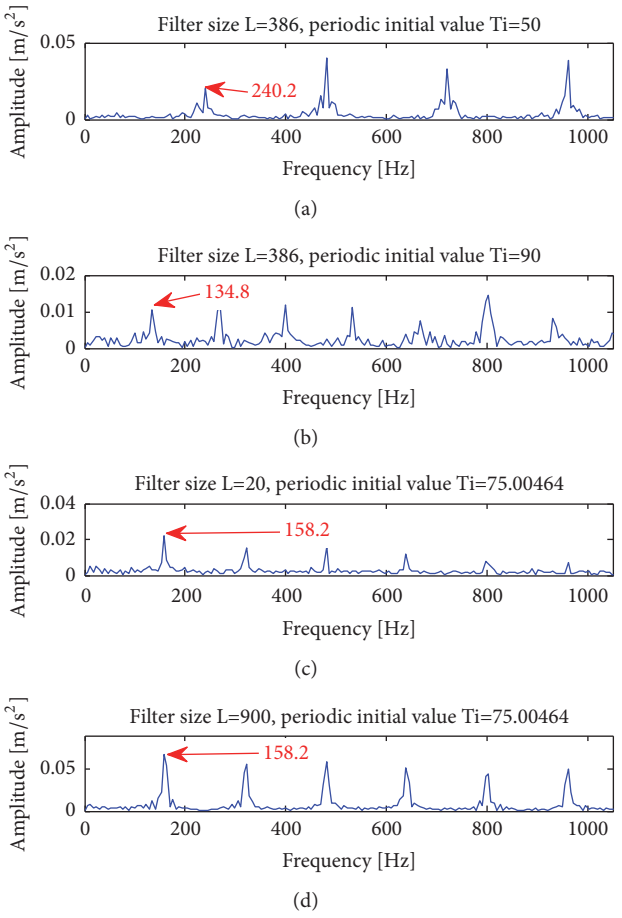

Figure 5: The effect of nonoptimal parameters on the results.

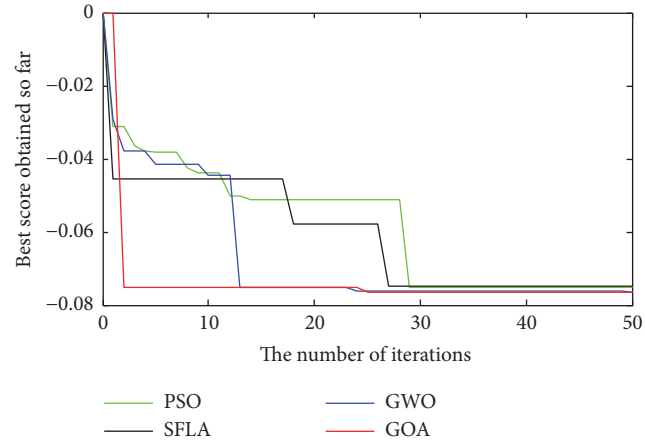

Figure 6: Convergence curves of optimization algorithms.

Figures 7(a) and 7(b), the characteristic frequencies obtained by MED are submerged in irrelevant frequency components. Although the frequency 158.2Hz and its harmonics obtained by MCKD can be observed, these frequencies are ambiguous due to the interference of irrelevant frequencies. Similarly, the frequency 159.2Hz and its harmonics can be obtained by FSK, but many interference frequencies exist in the envelope spectrum. From the comparison between Figures 4 and 7, the proposed approach has an outstanding advantage in the feature extraction of the noisy signal.

5. Case Studies

5.1. Case 1: Vibration Signal Analysis of CWRU Bearings. The data are derived from CWRU bearing dataset [40]. The bearing test rig is given in Figure 8 [44], and it is composed of four parts: a 2 hp motor, a decoder or a torque sensor, a dynamometer, and a controller. The sensors are fixed on the motor, and the motor speed is 1797rpm (the rotational frequency f_r = 1797/60Hz = 29.95Hz), the 6205-2RSJEMSKF bearing parameters are listed in Table 2. The sampling frequency $fs = 12KHz$, and the experimental data length $N = 2048$. We use the inner ring, outer ring, and rolling element signals to prove the feasibility of the proposed approach. The fault diameter of these three bearing components is 0.007 inches (0.01778 cm). Based on the parameters listed in Table 2 and the formulas in literature [45], we can calculate the corresponding characteristic frequencies and they are listed in Table 3.

5.1.1. Parameter Initialization. The parameters of MOMEDA include filter size L, window function *Window*, periodic initial value T_i, and periodic final value T_f. Next, we discuss the effect of different parameters on the MKurt of the filtered signal. The effect of window function on MKurt is not discussed in this paper, and we use a rectangular window in all the tests [28].

The approximate range of MOMEDA parameters can be determined according to the signal characteristics. Firstly, the FIR filters with different filter size L are constructed, the range of filter size is $L \in [1, 800]$, and the period interval is $T = [60 : 0.1 : 300]$ ($T_i = 60, T_f = 300$). Then, the periodic impacts are extracted from the different fault signals by these filters. Finally, the MKurt of these impact signals is obtained, and the results are shown in Figure 9.

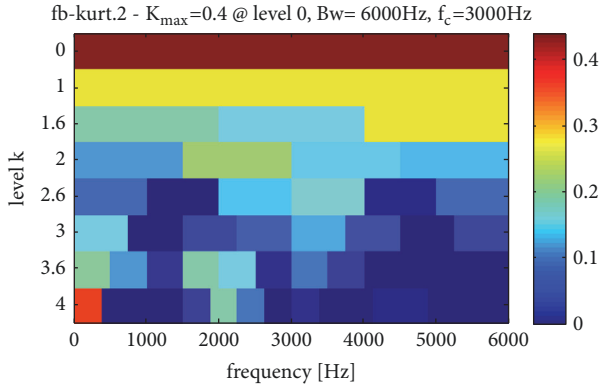

(a) Kurtogram analysis of the noisy signal

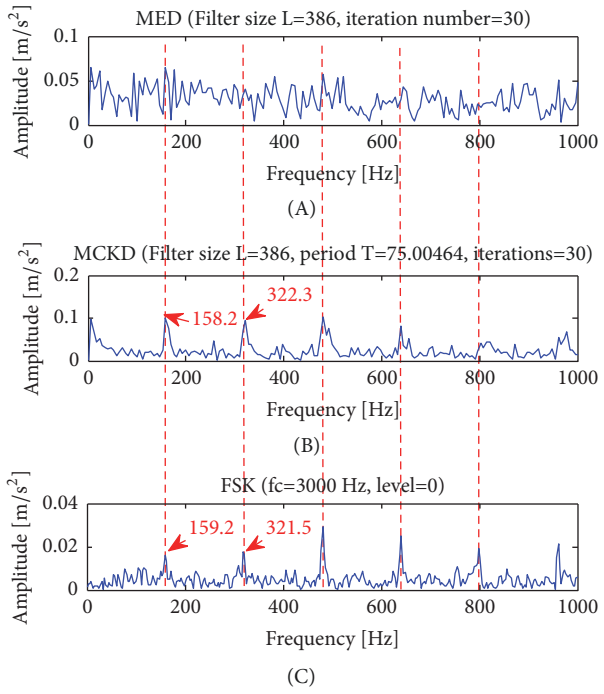

(b) The envelope analysis of impact signals obtained by MED, MCKD, and FSK

Figure 7: Comparison of feature extraction methods for the noisy signal.

The following conclusions can be drawn: (1) The MKurt of the filtered signals increases with the increase of the filter size L. However, none of the four MKurt curves is strictly monotone increasing function, and the local feature of these MKurt curves is irregular. Therefore, the filter with a larger filter size is not necessarily the optimal filter. (2) The MKurt of filtered signals in different fault states is different. Therefore, MKurt can characterize the characteristics of different fault signals. (3) When the range of filter size is $L \leq 500$, the three health statuses of bearings can be effectively distinguished by calculating the MKurt of the filtered signal. If the filter size is too large, some information of the periodic impact signal may be removed and the length of the filtered signal $(N - L + 1)$ becomes shorter. In addition, the deconvolution efficiency of MOMEDA is reduced, and the efficiency of parameter

Table 2: The SKF 6205 bearing parameters.

Ball diameter (d)	Number of balls (N)	Pitch diameter (D)	Contact angle (α)
7.938mm	9	39mm	0

Table 3: Characteristic frequencies.

Inner ring	Outer ring	Rolling element
162.1852Hz	107.3648Hz	141.1693Hz

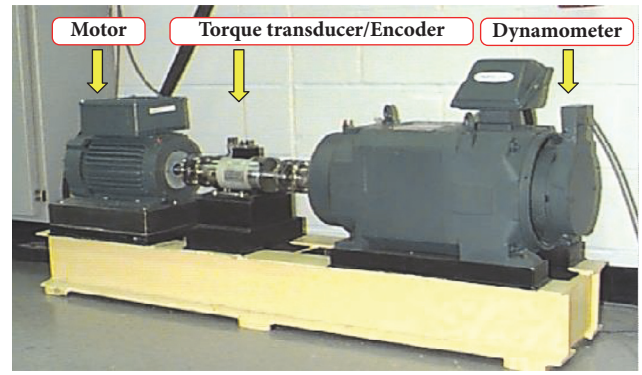

Figure 8: Bearing test rig.

optimization is also reduced. Therefore, the range of filter sizes is $L \in [1, 500]$ in this experiment.

Then, we analyze the effect of the periodic initial value T_i on the MKurt of the filtered signal. Firstly, the FIR filters with different T_i are constructed, the range of T_i is $T_i \in [5, 200]$, the periodic final value is $T_f = 400$, and the filter size is $L = 400$. Then, the periodic impacts are extracted from the different fault signals by these filters. Finally, the MKurt of these impact signals is obtained, and the results are shown in Figure 10.

The following conclusions can be drawn: (1) With the increase of T_i, the change of MKurt is irregular. (2) The MKurt of the filtered signal is large when T_i is small, the reason is that the high-frequency noise and high harmonics of the fault frequencies are mixed into the filtered signal. It can be seen that a filter with a large T_i can remove the high-frequency noise. Therefore, the range of T_i is $T_i \in [50, 150]$ in this experiment.

Then, we analyze the effect of the periodic final value T_f on the MKurt of the filtered signal. Firstly, the FIR filters with different T_f are constructed, the range of T_f is $T_f \in [200, 600]$, the periodic initial value is $T_i = 60$, and the filter size is $L = 400$. Then, the periodic impacts are extracted from the different fault signals by these filters. Finally, the MKurt of these impact signals is obtained, and the results are shown in Figure 11.

The results show that the periodic final value T_f does not affect the filtering results. Therefore, the optimization of the T_f is not necessary, and the final value $T_f = 400$ is used for all experiments. In summary, the number of search agents $S_{An} = 300$, the maximum number of iterations $M = 10$, the range

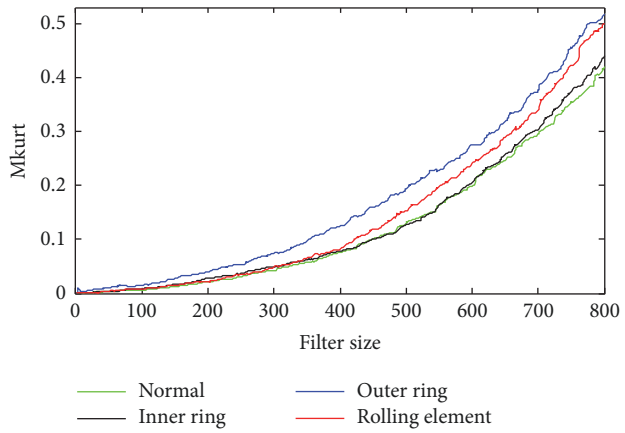

Figure 9: The relationship between MKurt and filter size.

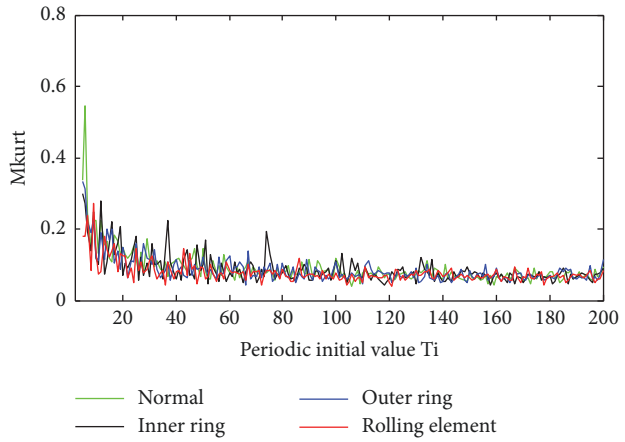

Figure 10: The relationship between MKurt and periodic initial value.

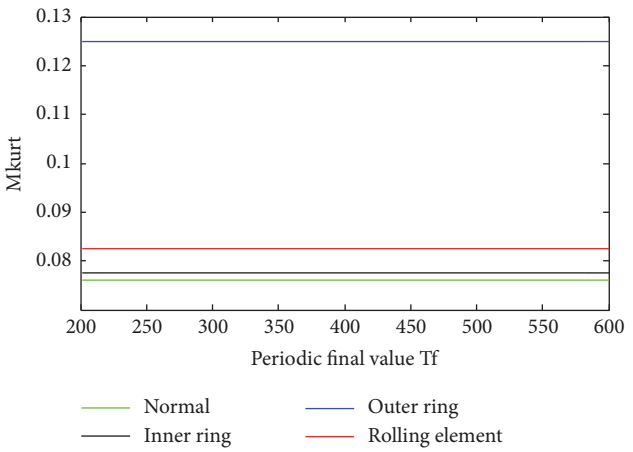

Figure 11: The relationship between MKurt and periodic final value.

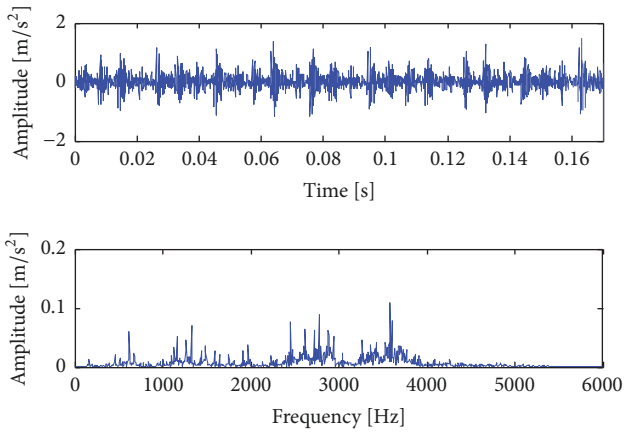

Figure 12: Inner ring signal and its frequency domain.

of filter size $L \in [1, 500]$, the range of periodic initial value $T_i \in [50, 150]$, and periodic final value $T_f = 400$.

5.1.2. Inner Ring Signal Analysis of CWRU Bearings. As shown in Figure 12, the waveforms of the inner ring signal have a certain regularity, which indicates that the rolling bearing has failed [44]. However, background noise and interference frequencies make it difficult to extract the inner ring fault characteristics directly from the frequency domain [2]. Therefore, we extract the inner ring fault features by using the proposed approach. Firstly, the parameters of the MOMEDA are optimized by GOA algorithm and the results are shown in Figure 13.

As shown in Figure 13, along with the increasing of iteration times, the grasshopper swarms tend to converge towards the best location, and the convergent curve gradually converges to the minimum. Meanwhile, a large number of particles are gathered at the right edge of Figure 13(a), and the results indicate that the optimal target may exist outside the range of the parameters. In order to ensure the efficiency of the algorithm and the filtering effect, we only consider the optimal solution of the algorithm when the filter size is less than or equal to 500. When the number of iterations $m = 9$, the MKurt ($MKurt = 0.2869$) is the maximum, and the optimal parameters $\gamma = (L, T_i) = (499, 74.15955)$ of MOMEDA are obtained.

Subsequently, the impact component in the inner ring signal is extracted by the optimized MOMEDA, and the envelope of the impact signal is given in Figure 14. When the frequencies are 164.1Hz and its multiples, several spectral peaks can be observed clearly. Moreover, these peak frequencies are approximate to the fault frequency (162.1852Hz) of inner ring and its harmonics. Due to the interference of transmission path and interference noise, there are some slight deviations between the measured values and the theoretical values. However, the proposed approach can effectively diagnose the inner ring fault.

In order to explore the effect of nonoptimal parameters on the results, we compared four sets of MOMEDA methods with fixed parameters. As shown in Figures 15(a) and 15(b), when the filter size L of MOMEDA is set to the optimal value $L = 499$ obtained by GOA and $T_i = 50$, the frequency 240.2Hz and its harmonics can be observed clearly. Meanwhile, when $T_i = 90$, the frequency 134.8Hz and its harmonics are obvious. However, the frequency 240.2 Hz is far greater than the characteristic frequency (162.1852Hz)

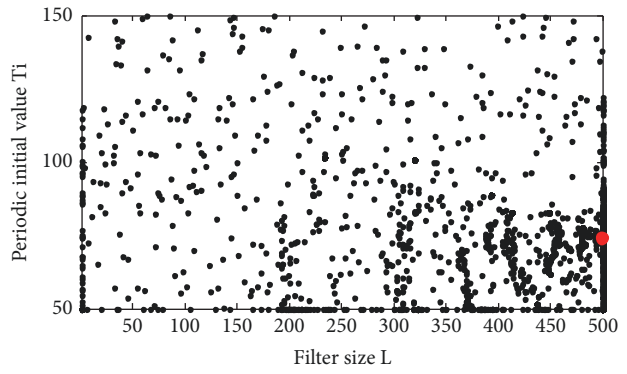

(a) The search history of grasshoppers

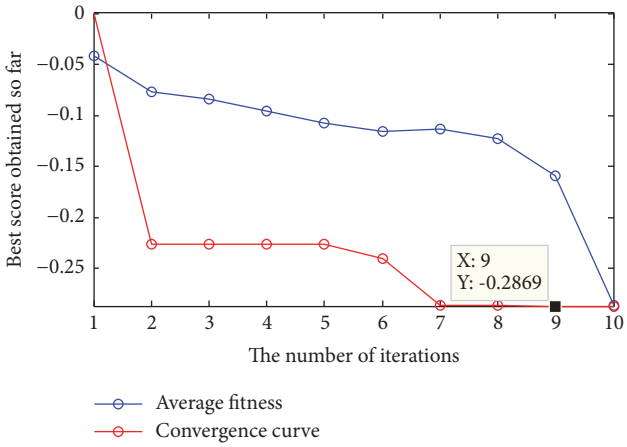

(b) Average fitness curve and convergence curve of GOA

FIGURE 13: Optimization results of MOMEDA obtained by GOA.

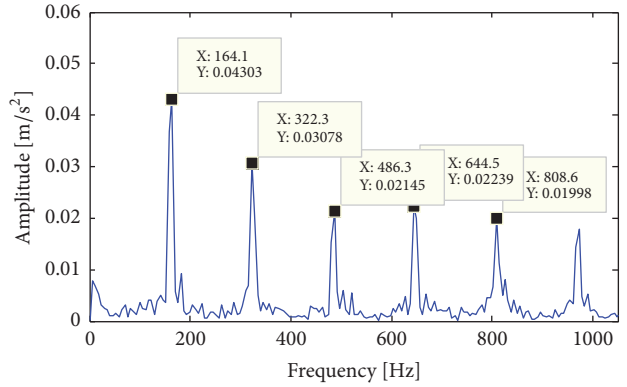

FIGURE 14: The envelope of the inner ring impact signal.

of inner ring, and 134.8 Hz is far less than the frequency. Therefore, the values of these two sets of parameters are not appropriate. As shown in Figure 15(c), when T_i of MOMEDA is set to the optimal value T_i = 74.15955 and L = 20, the frequency 164.1Hz and its second harmonic can be observed clearly. However, the envelope spectrum is disturbed by noise, and its high-order harmonics are not obvious. Therefore, if the filter size L of MOMEDA is too small, the noise in the signal cannot be removed effectively, and the satisfactory

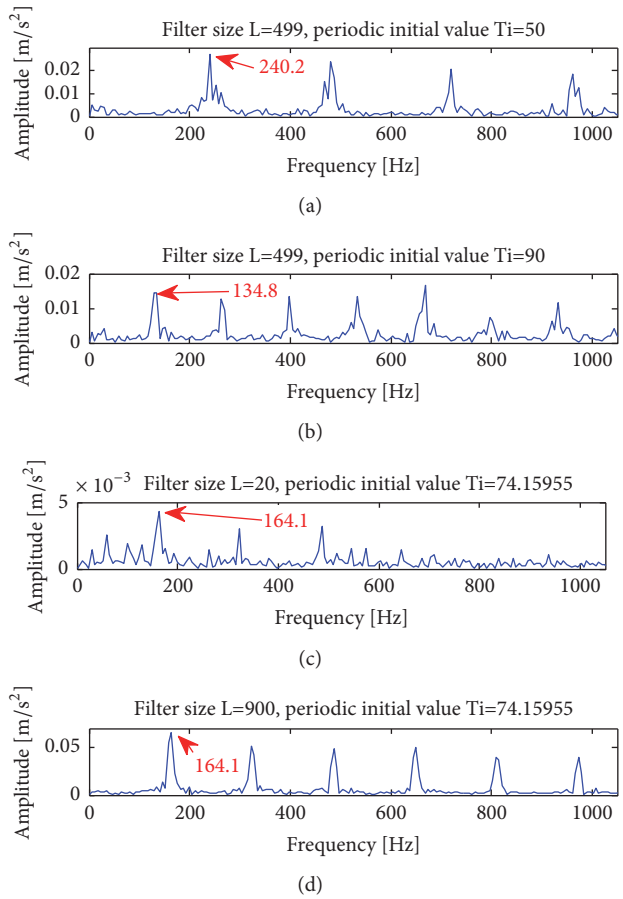

(a)

(b)

(c)

(d)

FIGURE 15: The effect of nonoptimal parameters on the results.

effect cannot be obtained. In Figure 15(d), the frequency 164.1Hz and its harmonics can be observed clearly when L = 900, and there is little interference around these harmonics. It can be seen that a better filtering effect can be obtained when the filter size L is larger. However, some information of the periodic impact signal may be removed when L is too large and the optimization process is time-consuming. We can draw a preliminary conclusion that the periodic initial value affects the size of the filtered signal characteristic frequency, and the filter size affects the noise reduction effect.

To demonstrate the preponderance of the approach, the method is compared with the methods with the optimal parameters, such as MED, MCKD, and FSK. Since the norms of MED, MCKD, and MOMEDA are based on kurtosis, the optimal filter size L = 499 obtained by GOA is used as the filter size of MED and MCKD, and the optimal periodic initial value T_i = 74.15955 is taken as the period of MCKD. The number of iterations of MED and MCKD is both set to 30. In view of the characteristic of the signal, the decomposition level of FSK is set to 3. As shown in Figure 16, the three methods MED, MCKD, and FSK can extract the inner ring fault frequency and its harmonics. However, the envelope spectra obtained by these three methods are disturbed by the irrelevant frequency components, and their harmonic envelopes are very blurred. Therefore, the proposed approach

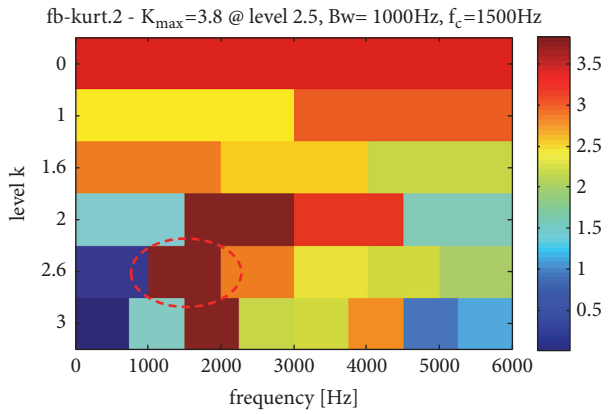

(a) Kurtogram analysis of the inner signal

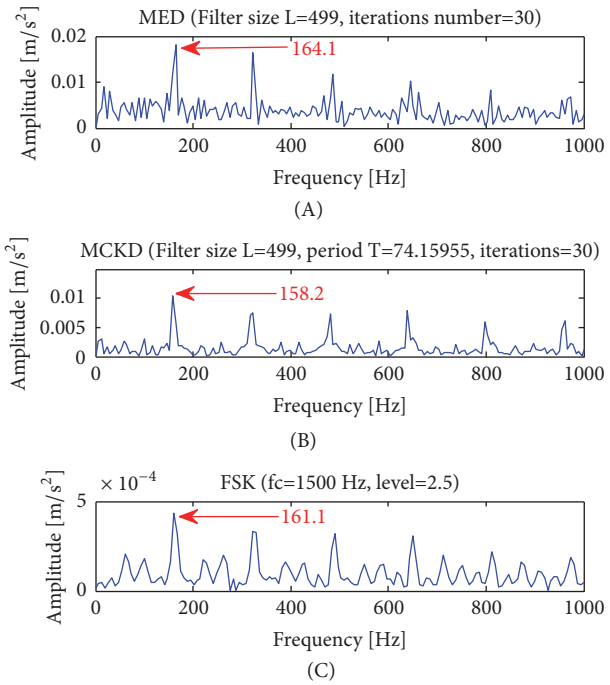

(b) The envelope analysis of impact signals obtained by MED, MCKD, and FSK

Figure 16: Comparison of feature extraction methods for the inner ring signal.

has outstanding performance in the feature extraction of the inner ring.

5.1.3. Outer Ring Signal Analysis of CWRU Bearings. As shown in Figure 17, the waveforms of the outer ring fault signal have a certain regularity, which indicates that the rolling bearing has failed. However, background noise and irrelevant components make it difficult to extract the outer ring fault characteristics directly from the frequency domain [2]. Therefore, we extract the outer ring fault features by using the proposed approach. Firstly, the parameters of the MOMEDA are optimized by GOA algorithm and the results are shown in Figure 18.

As shown in Figures 18(a) and 18(b), along with the increasing of iteration times, the grasshopper swarms tend to

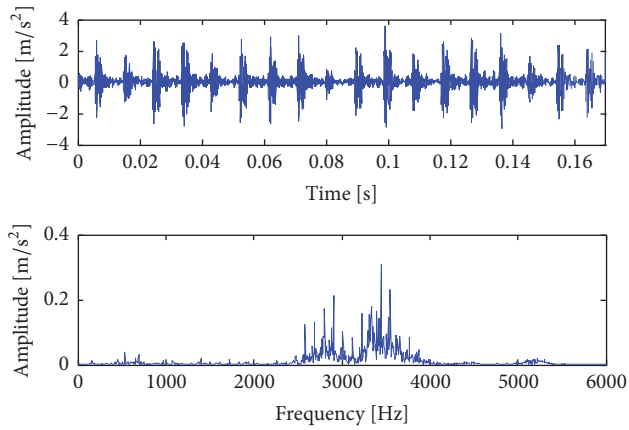

Figure 17: Outer ring signal and its frequency domain.

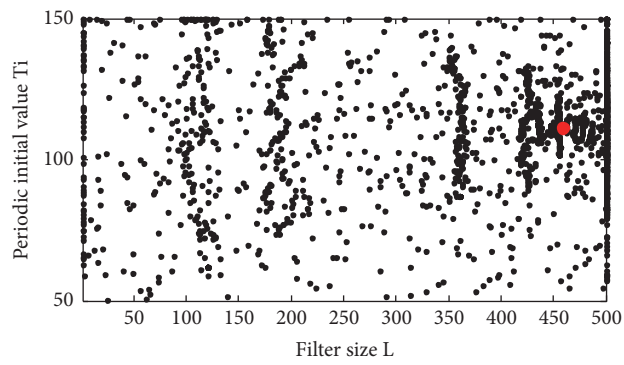

(a) The search history of grasshoppers

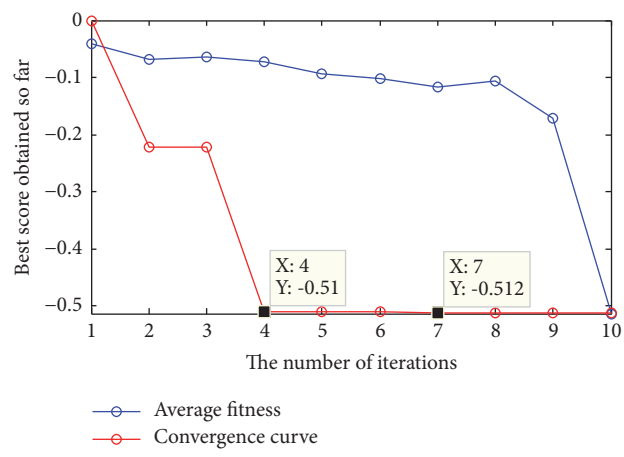

(b) Average fitness curve and convergence curve of GOA

Figure 18: Optimization results of MOMEDA obtained by GOA.

converge towards the best location, and the convergent curve gradually converges to the minimum. When the number of iterations $m = 7$, the MKurt ($MKurt = 0.5128$) is the maximum, and the optimal parameters $\gamma = (L, T_i) = (459, 111.4268)$ of MOMEDA are obtained.

Then, the impact component in the outer ring signal is extracted by the optimized MOMEDA, and the envelope of the impact signal is given in Figure 19. When the frequencies are 105.5Hz and its multiples, several spectral peaks can

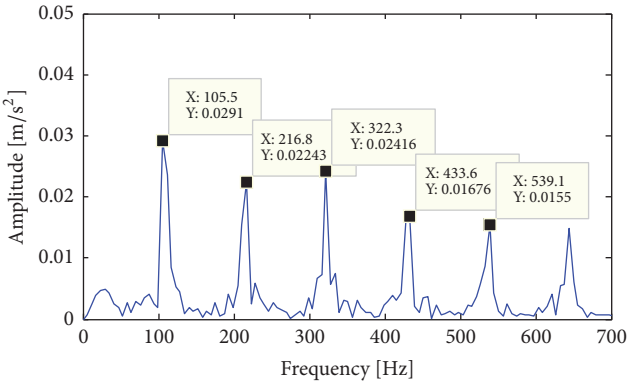

Figure 19: The envelope of the outer ring impact signal.

be observed clearly. Moreover, these peak frequencies are approximate to the characteristic frequency (107.3648Hz) of outer ring and its harmonics. Due to the influence of interference noise, there are some slight deviations between the measured values and the theoretical values. However, the proposed approach can effectively diagnose the outer ring fault of the bearing.

To explore the impact of nonoptimal parameters on the results, we compared four sets of MOMEDA methods with fixed parameters. As shown in Figures 20(a) and 20(b), when the filter size L of MOMEDA is set to the optimal value $L = 459$ obtained by GOA, $T_i = 50$ or $T_i = 90$, the frequencies 240.2Hz, 134.8Hz, and their harmonics can be observed clearly. However, these frequencies are far greater than the characteristic frequency (107.3648Hz) of outer ring and its harmonics. Therefore, the values of these two sets of parameters are not appropriate. As shown in Figure 20(c), when T_i of MOMEDA is set to the optimal value $T_i = 111.4268$ and $L = 20$, the frequency 105.5Hz can be observed clearly. However, the envelope spectrum is disturbed by noise, and its harmonics are submerged by interference frequency components. Therefore, the feature extraction method will fail when the filter size is too small. In Figure 20(d), 105.5Hz and its harmonics can be observed clearly when $L = 900$, and there is little interference frequency around these harmonics. It can be seen that a better filtering effect can be obtained when the filter size is larger. However, some information of the periodic impact signal may be removed when L is too large and the optimization process is time-consuming. Meanwhile, the larger the periodic initial value, the smaller the characteristic frequency of the filtered signal obtained by MOMEDA.

To demonstrate the superiority of the approach, the method is compared with the methods MED, MCKD, and FSK with the optimal parameters. The optimal filter size $L = 459$ obtained by GOA is used as the filter size of MED and MCKD, and the optimal periodic initial value $T_i = 111.4268$ is taken as the period of MCKD. The number of iterations of MED and MCKD is both set to 30. According to the characteristic of the outer ring signal, the decomposition level of FSK is set to 4. As shown in Figure 21, the three methods MED, MCKD, and FSK can extract the

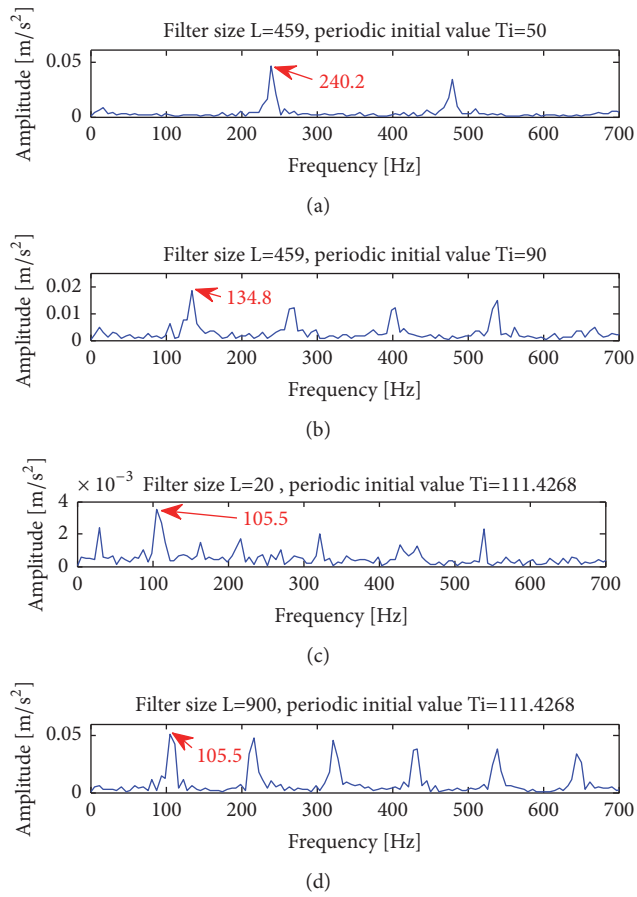

Figure 20: The effect of nonoptimal parameters on the results.

characteristic frequency of outer ring and its harmonics. However, the envelope obtained by MED contains many interference frequencies. For the outer ring, MCKD, FSK, and the proposed approach can achieve good results.

5.1.4. Rolling Element Signal Analysis of CWRU Bearings. According to the theory of Kumar et al. [46], when the rolling element fails, the frequency spectrum contains the second harmonic of the spin frequency. The spin frequency of the rolling element is generated by impacting the inner ring or outer ring. In general, the rolling element rotates once and it produces two impacts. Therefore, the characteristic frequency of the rolling element usually submerged in interference frequencies. Ma et al. [44] also proved that the proposed demodulation approach can obtain good results in the feature extraction of the inner ring and outer ring, but it has a poor effect in the feature extraction of the rolling element.

As shown in Figure 22, the regularity and periodicity of the waveforms are not obvious, and the frequencies contained in frequency domain waveform are more complex. In addition, the interference frequencies and noise make it difficult to extract fault features directly from frequency domain. Therefore, we extract the fault features by using the proposed approach. Firstly, the parameters of MOMEDA are optimized by GOA algorithm and the results are shown in Figure 23.

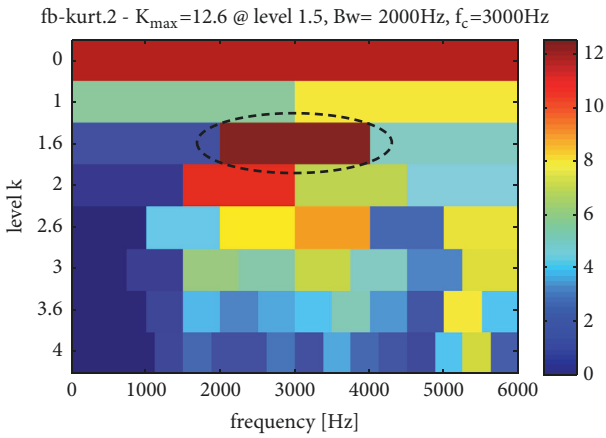

(a) Kurtogram analysis of the outer ring signal

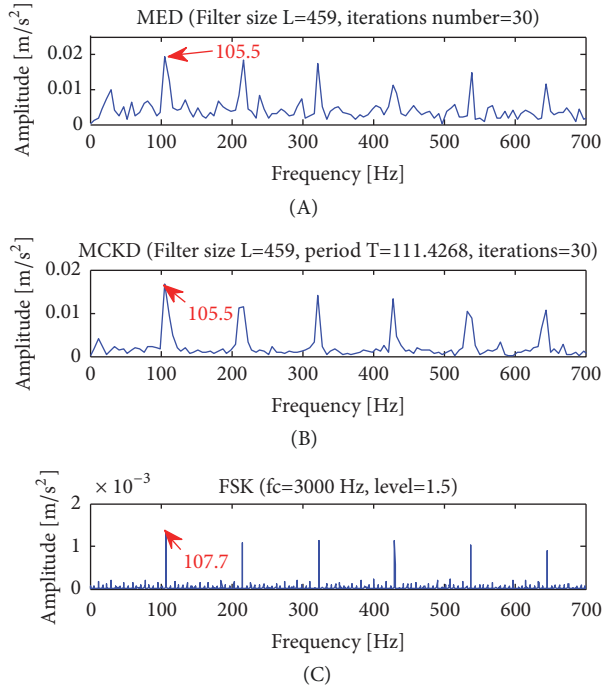

(b) The envelope analysis of impact signals obtained by MED, MCKD, and FSK

Figure 21: Comparison of feature extraction methods for the outer ring signal.

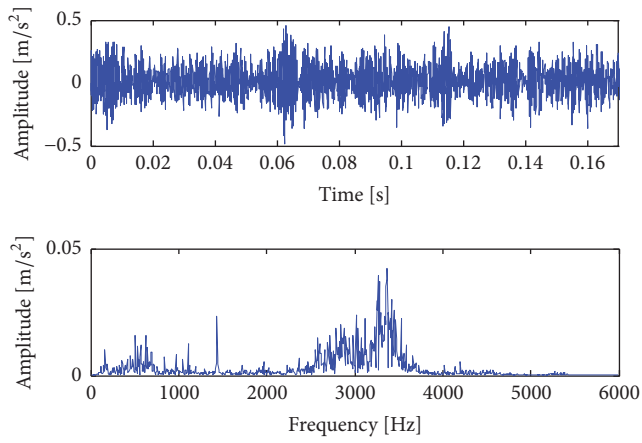

Figure 22: Rolling element signal and frequency domain.

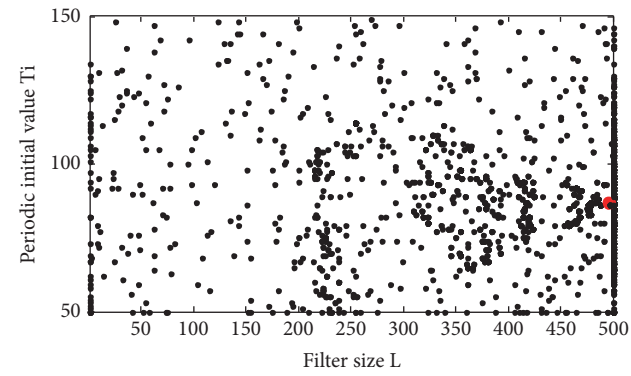

(a) The search history of grasshoppers

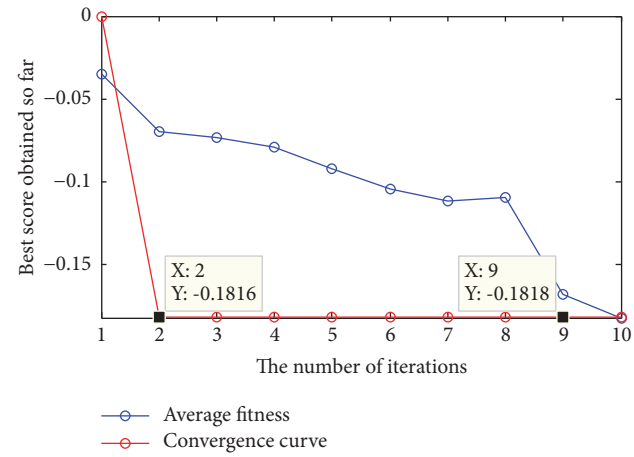

(b) Average fitness curve and convergence curve of GOA

Figure 23: Optimization results of MOMEDA obtained by GOA.

As shown in Figure 23, along with the increasing of iteration times, the grasshopper swarms tend to converge towards the best location, and the convergent curve gradually converges to the minimum. When the number of iterations $m = 9$, the MKurt ($MKurt = 0.18179$) is the maximum, and the optimal parameters $\gamma = (L, T_i) = (494, 85.5723)$ of MOMEDA are obtained. Then, the impact component in the rolling element signal is extracted by the optimized MOMEDA, and the envelope of the impact signal is given in Figure 24. When the frequencies are 140.6Hz and its multiples, several spectral peaks can be observed clearly. Moreover, these peak frequencies are close to the characteristic frequency (141.1693Hz) of rolling element and its harmonics. Due to the effect of interference noise, there are some slight deviations between the measured values and the theoretical values. However, the rolling element fault of the bearing can be identified accurately by the proposed approach.

To explore the impact of nonoptimal parameters on the results, we compared four sets of MOMEDA methods with fixed parameters. As shown in Figures 25(a) and 25(b), when the filter size L of MOMEDA is the optimal value $L = 494$

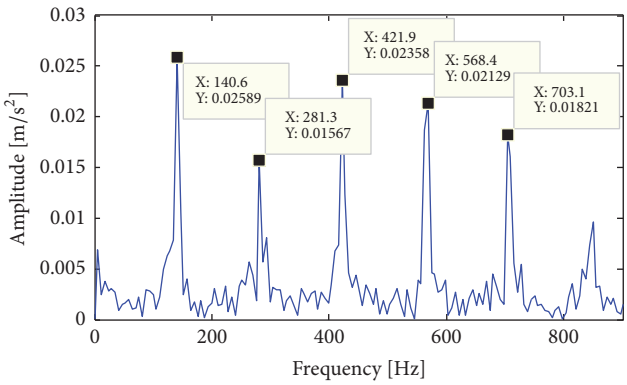

Figure 24: The envelope of the rolling element impact signal.

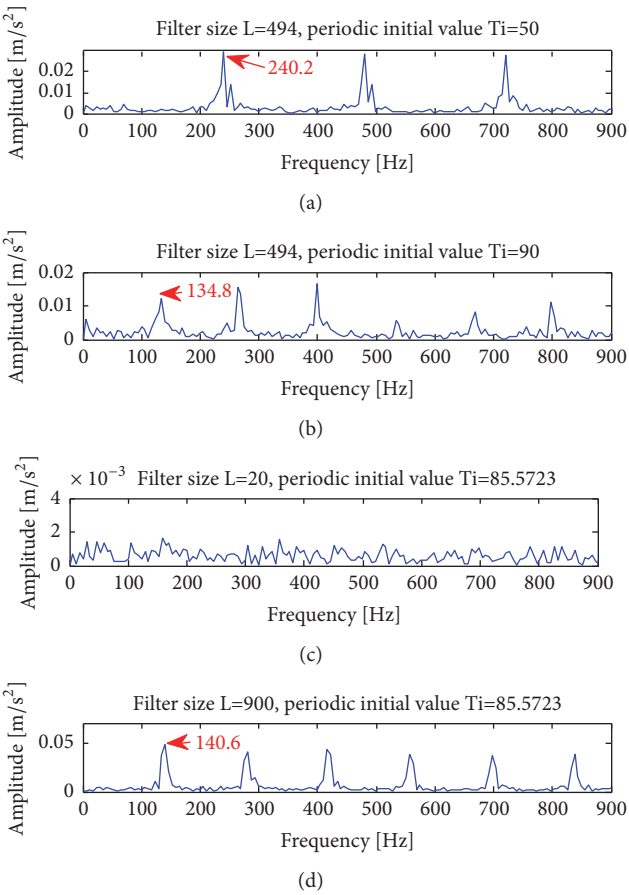

Figure 25: The effect of nonoptimal parameters on the results.

obtained by GOA and $T_i = 50$, the frequency 240.2Hz and its harmonics can be observed clearly. Meanwhile, when $T_i = 90$, the frequency 134.8Hz and its harmonics are obvious. However, these two frequencies and their harmonics are independent of the fault characteristic frequency. Therefore, the values of these two sets of parameters are not appropriate. As shown in Figure 25(c), when T_i of MOMEDA is set to the optimal value $T_i = 85.5723$ and $L = 20$, the effective frequency is submerged by the interference frequencies and the fault features cannot be extracted. So, if the filter size is too small, the noise in the signal cannot be effectively removed, and the feature extraction method will completely fail. In Figure 25(d), 140.6Hz and its harmonics can be observed clearly when $L = 900$. To sum up, the feature extraction method will fail when the periodic initial value T_i is not appropriate. In general, the larger T_i, the smaller the characteristic frequency of the filtered signal. The filter size L affects the noise reduction effect; if L is too small, the interference frequencies and noise in the signal cannot be removed effectively.

Table 4: The Rexnord ZA-2115 bearing parameters.

Ball diameter (d)	Number of balls (Z)	Pitch diameter (D)	Contact angle (α)
8.407 mm	16	71.501 mm	15.17

To demonstrate the superiority of the approach, the method is compared with the methods MED, MCKD, and FSK with the optimal parameters. The optimal filter size $L = 494$ obtained by GOA is used as the filter size of MED and MCKD, and the optimal periodic initial value $T_i = 85.5723$ is taken as the period of MCKD. The number of iterations of MED and MCKD is both set to 30. According to the characteristics of the rolling element signal, the decomposition level of FSK is set to 4. As shown in Figure 26, the envelope spectra obtained by MED, MCKD, and FSK all contain a large number of unrelated frequency components, and the effective frequencies are all submerged in the interference frequencies. For the rolling element signal, the above three feature extraction methods cannot achieve satisfactory results. Therefore, it is particularly difficult to extract the rolling element characteristic frequency compared with the inner ring and outer ring. However, the proposed method still achieves good results in the feature extraction of the rolling element.

5.2. Case 2: Vibration Signal Analysis of NASA Bearings. To verify the universality and reliability of the proposed approach, we analyze the NASA bearing dataset [41] by using the proposed approach. Figure 27 shows the test platform [47] of NASA, and four lubricated Rexnord ZA-2115 bearings are fixed on the spindle of the test rig. The spindle rotates under the drive of the motor, and its speed is 2000 rpm. Therefore, the rotating frequency of the bearing is 33.33 Hz ($f_r = 2000/60 = 33.33$ Hz). The PCB353B33 acceleration sensors are fixed on the bearing housing, and the signals are collected by NI DAQ Card 6062E data acquisition card. The data length $N = 20480$ and the sampling frequency $f_s = 20$KHz. In this experiment, the inner ring signal comes from Bearing 3 of No. 1 dataset, the outer ring signal comes from Bearing 1 of No. 2 dataset, the rolling element signal comes from Bearing 3 of No. 1 dataset, and the data length is 2048. The parameters of Rexnord ZA-2115 bearing are listed in Table 4. Based on the parameters listed in Table 4 and the formulas in literature [45], we can calculate the corresponding characteristic frequencies and they are listed in Table 5.

Table 5: Characteristic frequencies.

Inner ring	Outer ring	Rolling element
296.91Hz	236.4Hz	139.9Hz

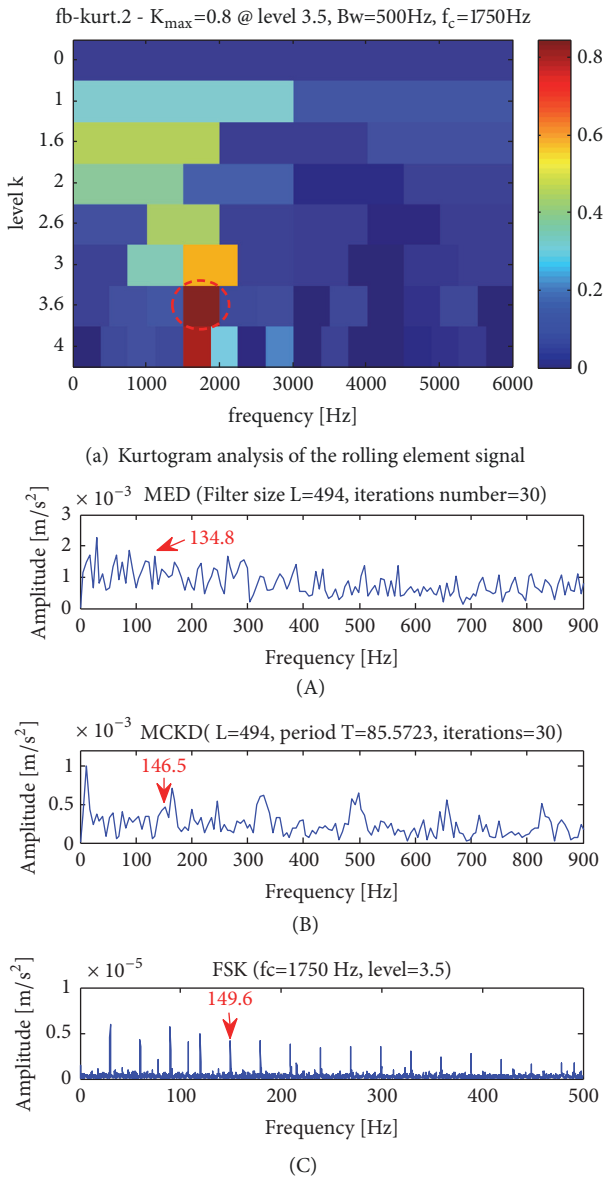

(b) The envelope analysis of impact signals obtained by MED, MCKD, and FSK

Figure 26: Comparison of feature extraction methods for the rolling element signal.

The structure and operation mode of bearings share some similarities, and the bearings vibration signals have a corresponding periodicity. Therefore, the initialization of parameters in this section is the same as that in Section 5.1.1.

5.2.1. Inner Ring Signal Analysis of NASA Bearings. As shown in Figure 28, due to the interference of interference frequencies and noise, it is difficult to extract the inner ring fault

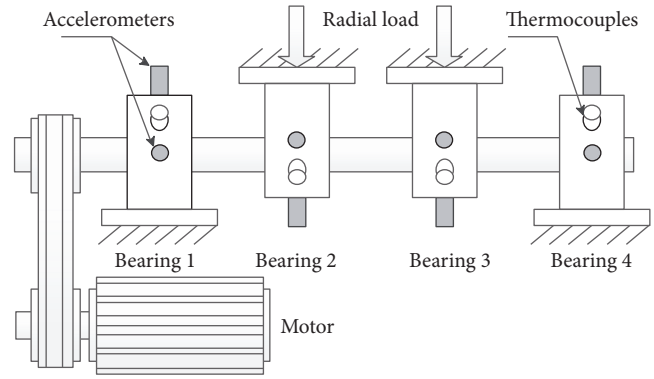

Figure 27: Bearing experiment platform.

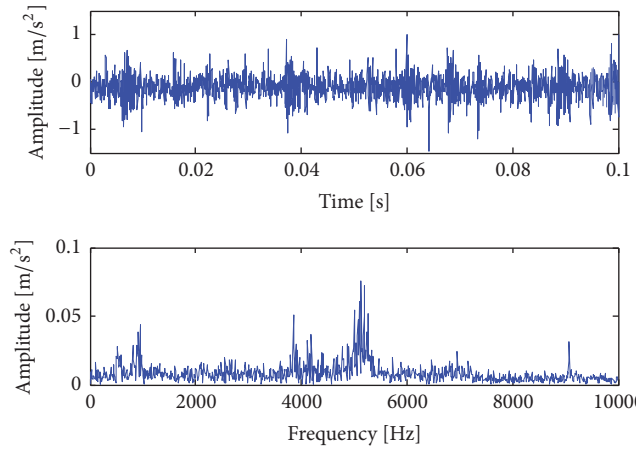

Figure 28: Inner ring signal and its frequency domain.

features. Therefore, we extract the inner ring fault features by using the proposed method. Firstly, the MOMEDA parameters are optimized by GOA algorithm.

As shown in Figure 29, along with the increasing of iteration times, the convergent curve gradually converges to the minimum. When the number of iterations $m = 3$, the MKurt ($MKurt = 0.2168$) is the maximum, and the optimal parameters $\gamma = (L, T_i) = (498, 67.7462)$ of MOMEDA are obtained. Then, the impact component in the inner ring signal is extracted by the optimized MOMEDA, and the envelope of the impact signal is given in Figure 30(d). When the frequencies are 293 Hz and its multiples, several spectral peaks can be observed clearly. Moreover, these peak frequencies are approximate to the characteristic frequency (296.91Hz) of inner ring and its harmonics. Due to the interference of background noise and transmission path, there are some slight deviations between the measured values and the theoretical values. However, the proposed approach can effectively diagnose the inner ring fault of the bearing.

To demonstrate the superiority of the approach, the method is compared with the methods with the optimal parameters, such as MED, MCKD, and FSK. Since the norms of MED, MCKD, and MOMEDA are based on kurtosis, the optimal filter size $L = 498$ obtained by GOA is used as the

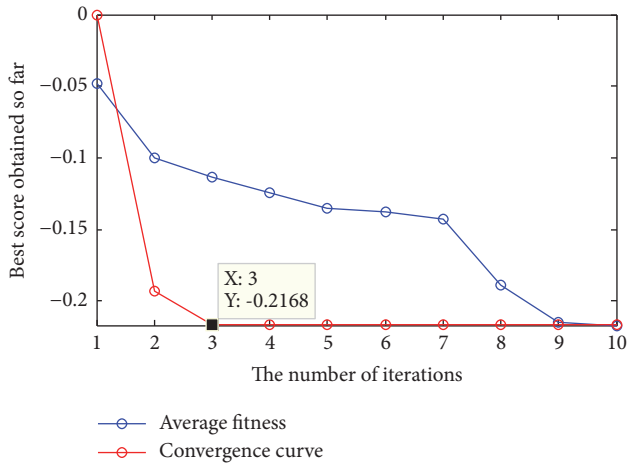

Figure 29: Optimization results of MOMEDA obtained by GOA.

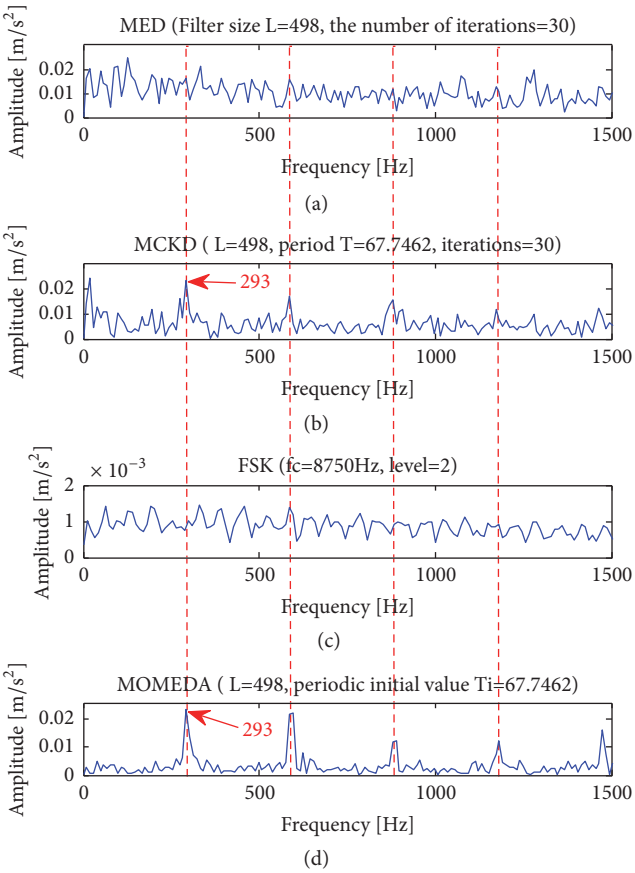

Figure 30: The envelope analysis of impact signals obtained by MED, MCKD, FSK, and MOMEDA.

filter size of MED and MCKD, and the optimal periodic initial value $T_i = 67.7462$ is taken as the period of MCKD. The number of iterations of MED and MCKD is both set to 30. In view of the characteristic of the signal, the decomposition level of FSK is set to 3. The kurtosis of the filtered signal obtained by FSK is maximum when the decomposition level is 2. At this point, the central frequency of the filtered signal

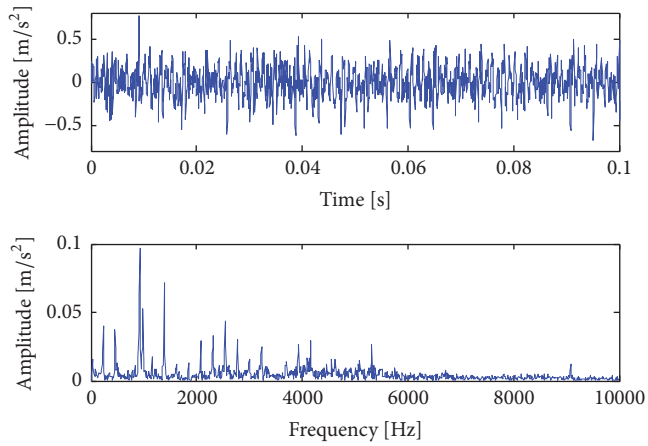

Figure 31: Outer ring signal and its frequency domain.

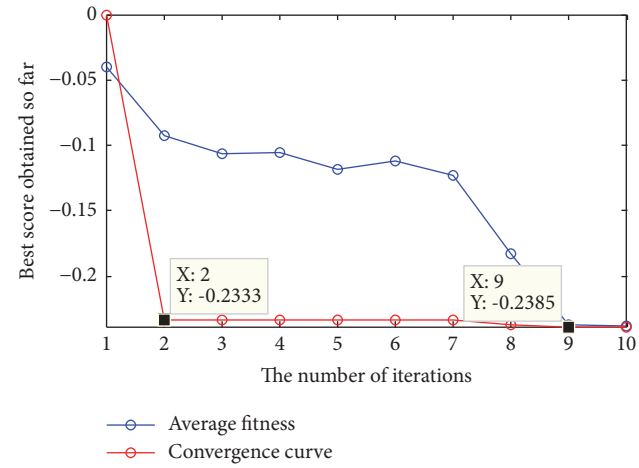

Figure 32: Optimization results of MOMEDA obtained by GOA.

is 8750Hz, the bandwidth is 2500Hz, and the envelope of the filtered signal is given in Figure 30(c). As shown in Figures 30(a) and 30(c), the envelope spectra obtained by MED and FSK are disturbed by many irrelevant frequencies, and it is unrealistic to extract the fault characteristic frequency. In Figure 30(b), although MCKD can extract the inner ring fault features, the frequency and its harmonics are disturbed by many irrelevant frequencies. Therefore, the proposed approach has outstanding advantages in the feature extraction of the inner ring.

5.2.2. Outer Ring Signal Analysis of NASA Bearings. As shown in Figure 31, although the waveforms have a certain regularity, it is difficult to extract fault features directly from the frequency domain. Therefore, we extract the outer ring fault features by using the proposed method. Firstly, the parameters of MOMEDA are optimized by GOA algorithm and the results are shown in Figure 32.

When the number of iterations $m = 9$, the MKurt ($Mkurt = 0.2385$) is the maximum, and the optimal parameters $\gamma = (L, T_i) = (496, 84.7148)$ of MOMEDA are obtained. Then, the impact component in the outer ring

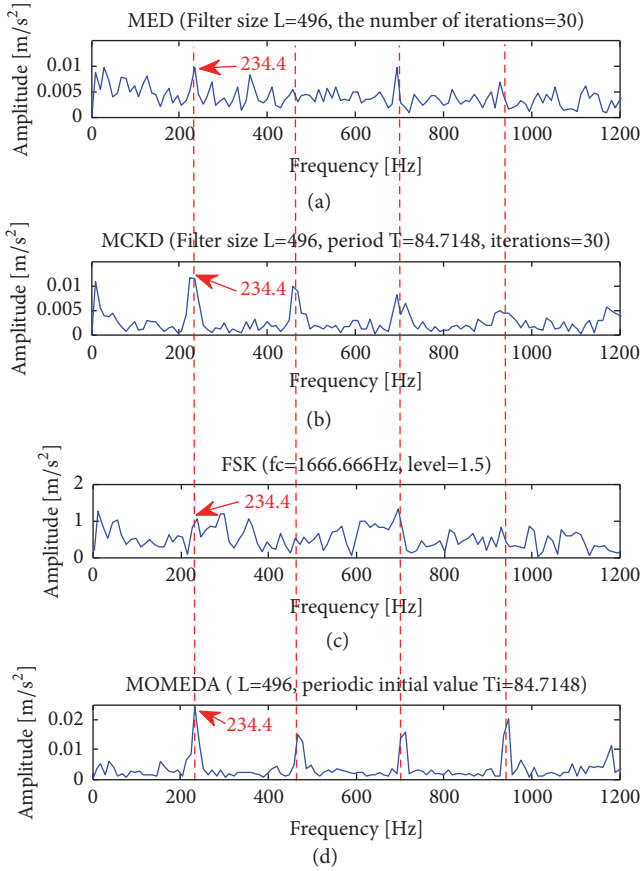

FIGURE 33: The envelope analysis of impact signals obtained by MED, MCKD, FSK, and MOMEDA.

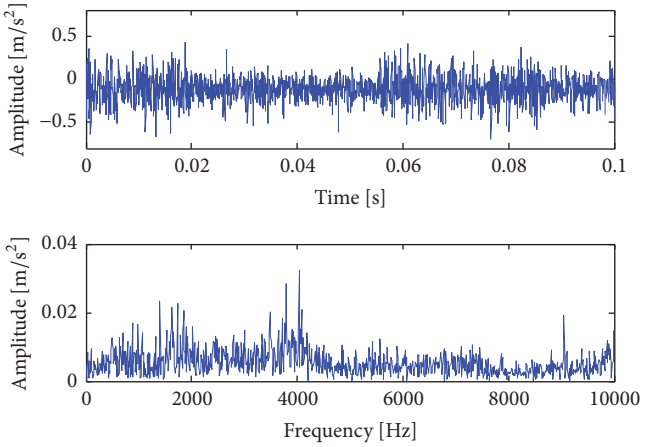

FIGURE 34: Rolling element signal and its frequency domain.

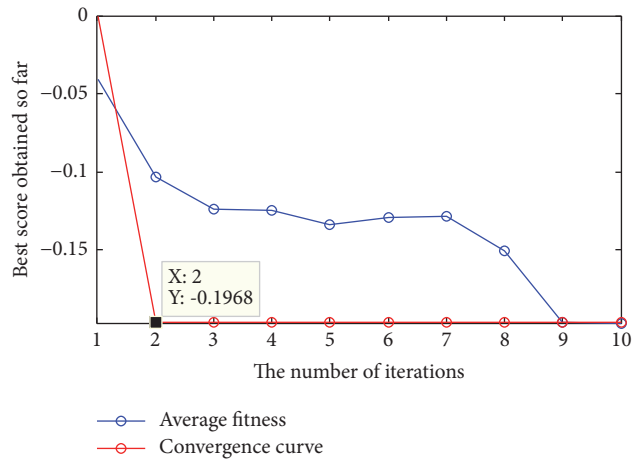

FIGURE 35: Optimization results of MOMEDA obtained by GOA.

signal is extracted by the optimized MOMEDA, and the envelope of the impact component is given in Figure 33(d). When the frequencies are 234.4Hz and its multiples, several spectral peaks can be observed clearly. Moreover, these peak frequencies are approximate to the outer ring characteristic frequency (236.4Hz) and its harmonics. Due to the interference of interference noise, there are slight deviations between the measured values and the theoretical values. However, the proposed approach can effectively diagnose the outer ring fault.

Then, we compared the proposed approach with the methods MED, MCKD, and FSK with the optimal parameters. The optimal filter size $L = 496$ obtained by GOA is used as the filter size of MED and MCKD, and the optimal periodic initial value $T_i = 84.7148$ is taken as the period of MCKD. The number of iterations of MED and MCKD is both set to 30, and the decomposition level of the FSK is set to 3. The kurtosis of the filtered signal obtained by FSK is maximum when the decomposition level is 1.5. At this point, the central frequency of the filtered signal is 1666.666Hz, the bandwidth is 3333.33Hz, and the envelope analysis of the filtered signal is shown in Figure 33(c). In Figures 33(a) and 33(c), the characteristic frequencies and their harmonics can be observed. However, these frequencies are disturbed by many interference frequencies. Therefore, it is difficult to identify the outer ring characteristic frequency through MED and FSK. In Figure 33(b), although MCKD can extract the outer ring characteristic frequency and its harmonics, the amplitudes of these harmonics are small and the spectral peaks are not obvious. Therefore, the proposed approach has outstanding performance in the feature extraction of the outer ring.

5.2.3. Rolling Element Signal Analysis of NASA Bearings. As shown in Figure 34, the regularity of the waveforms is not significant, and the frequencies contained in the frequency domain waveform are more complex. In addition, the interference frequencies and noise make it difficult to extract fault features directly from frequency domain. Therefore, we extract the fault features by the proposed approach. Firstly, the parameters of MOMEDA are optimized by GOA algorithm and the results are shown in Figure 35.

As shown in Figure 35, when the number of iterations $m = 2$, the MKurt ($Mkurt = 0.19684$) is the maximum, and the optimal parameters $\gamma = (L, T_i) = (500, 143.0353)$ of MOMEDA are obtained. Then, the impact component is extracted by the optimized MOMEDA, and the envelope

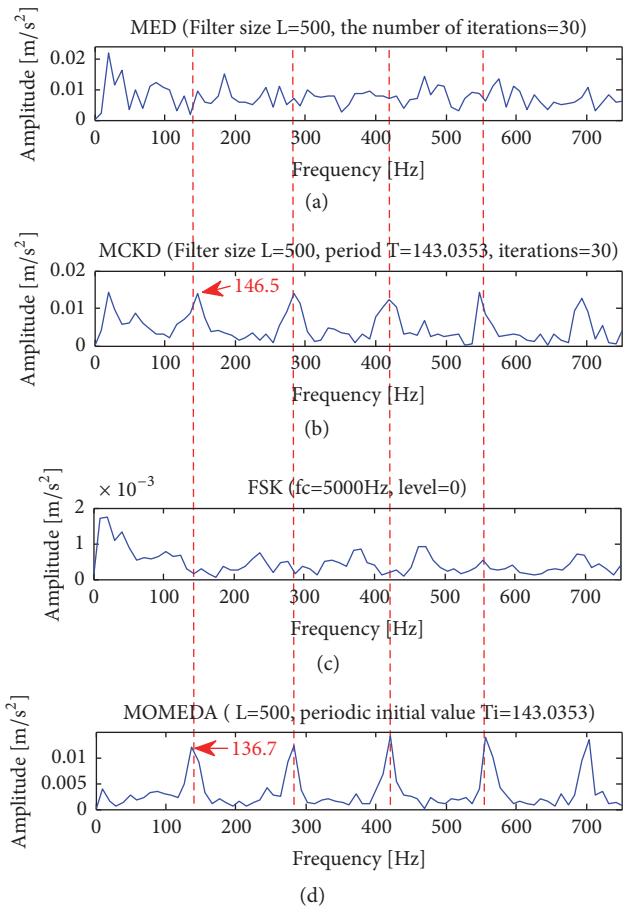

FIGURE 36: The envelope analysis of impact signals obtained by MED, MCKD, FSK, and MOMEDA.

of the impact signal is given in Figure 36(d). When the frequencies are 136.7Hz and its multiples, several spectral peaks can be observed clearly. Moreover, these peak frequencies are approximate to the characteristic frequency (139.9Hz) of rolling element and its harmonics. Due to the interference of background noise and transmission path, there are some slight deviations between the measured values and the theoretical values. However, the proposed approach can effectively diagnose the rolling element fault.

Then, the proposed method is compared with the methods MED, MCKD, and FSK with the optimal parameters. The optimal filter size $L = 500$ obtained by GOA is used as the filter size of MED and MCKD, and the optimal period initial value $T_i = 143.0353$ is taken as the period of MCKD. The number of iterations of MED and MCKD is both set to 30, and the decomposition level of FSK is set to 3. The kurtosis of the filtered signal obtained by FSK is maximum when the decomposition level is 0. At this point, the central frequency of the filtered signal is 5000Hz, the bandwidth is 10000Hz, and the envelope of the filtered signal is given in Figure 36(c). As shown in Figures 36(a) and 36(c), the envelope spectra obtained by MED and FSK are disturbed by many irrelevant frequencies, and it is difficult to extract the rolling element characteristic frequency through MED and FSK. In Figure 36(b), although MCKD can extract the characteristic frequency, the deviation between the peak frequency (146.5Hz) and fault characteristic frequency (136.7Hz) is large. Therefore, the proposed approach has excellent performance in the feature extraction of the rolling element.

6. Discussions

Through the comparison and analysis of several sets of experiments, the effectiveness and significant advantages of the proposed method are proved. The experimental process and preliminary conclusions of this paper are discussed below.

(1) It can be seen from the analysis of the simulation signal that MED, MCKD, and FSK cannot achieve satisfactory results in noisy environments. However, the characteristic frequencies contained in the noisy signal can be extracted effectively by the proposed approach. By analyzing the bearing signals come from two different experimental platforms, the results show that the fault features of the inner ring and outer ring are obvious, and the fault features are easy to be extracted. The rolling element with local damage periodically hits the inner ring and outer ring, which leads to the coupling effect between the inner and outer ring [44]. In addition, the rolling element vibration signal is affected by background noise and interference components. Therefore, the feature extraction of the rolling element is difficult and the characteristic frequency is not obvious. Nevertheless, the proposed method still achieves the desired effect, and the validity and reliability of the method are verified.

(2) It is known from the parameter initialization that the filter size is positively correlated with the MKurt of the filtered signal, but the MKurt curve is not a strictly monotone increasing curve. Therefore, there is a local optimal solution for the filter size. In addition, the change of MKurt is irregular when the periodic initial value changes, so the parameter optimization is very difficult. It is known from the experiments with fixed parameters that a large amount of noise and interference is removed when the filter size is large, and the envelope spectra are clear. However, the efficiency of the algorithm is very low when the filter size is too large, and the fault impact signal may be removed. The larger the periodic initial value is, the smaller the characteristic frequency extracted from the filtered signal is. Comparison experiments of optimization algorithms show that GOA method is not only simple in calculation, but also high in convergent speed and accuracy. From the optimization process of GOA, it is known that the grasshoppers are widely distributed in the whole search space at the beginning of iteration, which ensures the global search scope. At the end of iteration, the grasshopper swarm approaches the optimal position and moves slowly, which ensures the local search accuracy. Therefore, the GOA algorithm guarantees the reliability of parameter optimization.

(3) The optimal parameters of MOMEDA obtained by GOA are used in MED and MCKD because these three deconvolution methods are all based on kurtosis norm. The experimental results demonstrate that MED is only suitable

for single impact signal. Meanwhile, the envelope spectrum obtained by MED contains a large number of interference frequencies. Although MCKD can extract a series of impact components from the noisy signal, the higher harmonics obtained by this method are often disturbed by irrelevant frequencies. In the process of processing the weak noise signal, FSK can achieve satisfactory results. However, when the signal contains strong background noise or interference frequencies, it is sometimes difficult to extract fault features through FSK. Therefore, for the above three methods, signal preprocessing is necessary before feature extraction. All signals have not been preprocessed in this paper, and the proposed method still achieves satisfactory results.

7. Conclusions

A parameter adaptive MOMEDA feature extraction method based on GOA is proposed for solving the problem of the bearing fault diagnosis. The GOA is introduced to determine the optimal parameters of MOMEDA. The algorithm has its own unique advantages, and it updates the position of individual search agent by involving all search agents. In addition, GOA can adaptively determine the optimal filter size and periodic initial value of MOMEDA based on the signal characteristics and effectively avoid the randomness of artificial adoption. The simulation signal and bearing signals from two different experimental platforms are analyzed by the proposed method, satisfactory feature extraction results can be obtained, and the validity and reliability of the method are verified. Therefore, several meaningful contributions of this paper are as follows: (a) the main parameters affecting the filtering results and feature extraction results are evaluated; (b) a new optimization model containing these influence parameters is constructed; (c) GOA is introduced to determine the appropriate MOMEDA parameters while extracting fault features. Through several case studies, some beneficial conclusions are gained.

(a) The effect of feature extraction is affected by the filter size and the periodic initial value, and the influences of these two parameters on the results are different. Therefore, these influencing factors must be considered comprehensively in the process of parameter optimization.

(b) The feature extraction effect of the proposed method is compared with that of MOMEDA with fixed parameters. The results show that the filter size affects the noise reduction effect, and the periodic initial value affects the size of the characteristic frequency.

(c) The proposed approach is compared with the three methods MED, MCKD, and FSK with optimal parameters. We found that the feature extraction effect of the proposed approach is better than that of the other three methods in all cases, and it meets the requirement of feature extraction for all fault types.

However, the damage problem of the bearing is complicated in the actual industrial production process, the fault impact signals are often submerged by noises, and the composite fault may occur. Therefore, we will collect bearing data from the industrial environment and analyze these data by the approach. In addition, the composite fault experiment and its analysis will be implemented step by step, and the proposed method is expected to address these complex issues.

Abbreviations

MED:	Minimum entropy deconvolution
MCKD:	Maximum correlated kurtosis deconvolution
FSK:	Fast spectral kurtosis
GOA:	Grasshopper optimization algorithm
MOMEDA:	Multipoint optimal minimum entropy deconvolution adjusted
MKurt:	Multipoint kurtosis
EMD:	Empirical mode decomposition
EEMD:	Ensemble empirical mode decomposition
CEEMDAN:	Complete ensemble empirical mode decomposition adaptive noise
PE:	Permutation entropy
LMD:	Local mean decomposition
ELMD:	Ensemble local mean decomposition
CELMD:	Complete ensemble local mean decomposition
VMD:	Variational mode decomposition
EWT:	Empirical wavelet transform
CA:	Cyclostationary analysis
SR:	Stochastic resonance
TEO:	Teager energy operator
CPF:	Combined product function
PF:	Product functions
CK:	Correlation kurtosis
PSO:	Particle swarm optimization
SFLA:	Shuffled frog leaping algorithm
BA:	Bat algorithm
FPA:	Flower pollination algorithm
CS:	Cuckoo search algorithm
SVM:	Support vector machine
CWRU:	Case Western Reserve University
NASA:	National Aeronautics and Space Administration
GWO:	Gray wolf optimization algorithm.

Data Availability

The data used to support the findings of this study are available from the corresponding author upon request.

Conflicts of Interest

The authors declare that there are no conflicts of interest regarding the publication of this paper.

Acknowledgments

This work is supported by the National Natural Science Foundation of China (nos. 61663017 and 51765022). The authors sincerely thank the team for their guidance and thank the Case West Reserve University and the University of Cincinnati for their bearing datasets.

References

[1] H. Yuan, J. Chen, and G. Dong, "Bearing Fault Diagnosis Based on Improved Locality-Constrained Linear Coding and Adaptive PSO-Optimized SVM," *Mathematical Problems in Engineering*, vol. 2017, Article ID 7257603, 16 pages, 2017.

[2] J. Ma, J. Wu, Y. Fan, and X. Wang, "The rolling bearing fault feature extraction based on the lmd and envelope demodulation," *Mathematical Problems in Engineering*, vol. 2015, Article ID 429185, 13 pages, 2015.

[3] M. R. Shahriar, P. Borghesani, R. B. Randall, and A. C. C. Tan, "An assessment of envelope-based demodulation in case of proximity of carrier and modulation frequencies," *Mechanical Systems and Signal Processing*, vol. 96, pp. 176–200, 2017.

[4] N. E. Huang, Z. Shen, and S. R. Long, "The empirical mode decomposition and the Hilbert spectrum for nonlinear and non-stationary time series analysis," *Proceedings Mathematical Physical & Engineering Sciences*, vol. 454, no. 1971, pp. 903–995, 1998.

[5] Z. H. Wu and N. E. Huang, "Ensemble empirical mode decomposition: a noise-assisted data analysis method," *Advances in Adaptive Data Analysis (AADA)*, vol. 1, no. 1, pp. 1–41, 2009.

[6] J. Helske and P. Luukko, "Ensemble empirical mode decomposition (EEMD) and its completevariant (CEEMDAN)," *International Journal of Public Health*, vol. 60, no. 5, pp. 1–9, 2016.

[7] S. Zhou, S. Qian, W. Chang, Y. Xiao, and Y. Cheng, "A Novel Bearing Multi-Fault Diagnosis Approach Based on Weighted Permutation Entropy and an Improved SVM Ensemble Classifier," *Sensors*, vol. 18, no. 6, p. 1934, 2018.

[8] Y. Lv, R. Yuan, T. Wang, H. Li, and G. Song, "Health degradation monitoring and early fault diagnosis of a rolling bearing based on CEEMDAN and improved MMSE," *Materials*, vol. 11, no. 6, Article ID ma11061009, 2018.

[9] J. S. Smith, "The local mean decomposition and its application to EEG perception data," *Journal of the Royal Society Interface*, vol. 2, no. 5, pp. 443–454, 2005.

[10] J. Cheng, "Ensemble local mean decomposition method based on noise-assisted analysis," *Journal of Mechanical Engineering*, vol. 47, no. 03, pp. 55–62, 2011.

[11] L. Wang, Z. Liu, Q. Miao, and X. Zhang, "Complete ensemble local mean decomposition with adaptive noise and its application to fault diagnosis for rolling bearings," *Mechanical Systems and Signal Processing*, vol. 106, pp. 24–39, 2018.

[12] L. Zhang, Z. Wang, and L. Quan, "Research on weak fault extraction method for alleviating the mode mixing of LMD," *Entropy*, vol. 20, no. 5, Article ID e20050387, 2018.

[13] L. Wang, Z. Liu, Q. Miao, and X. Zhang, "Time–frequency analysis based on ensemble local mean decomposition and fast kurtogram for rotating machinery fault diagnosis," *Mechanical Systems and Signal Processing*, vol. 103, pp. 60–75, 2018.

[14] K. Dragomiretskiy and D. Zosso, "Variational mode decomposition," *IEEE Transactions on Signal Processing*, vol. 62, no. 3, pp. 531–544, 2014.

[15] J. Gilles, "Empirical wavelet transform," *IEEE Transactions on Signal Processing*, vol. 61, no. 16, pp. 3999–4010, 2013.

[16] Z. Wang, J. Wang, and W. Du, "Research on Fault Diagnosis of Gearbox with Improved Variational Mode Decomposition," *Sensors*, vol. 18, no. 10, Article ID s18103510, 2018.

[17] X. Zhang, Q. Miao, H. Zhang, and L. Wang, "A parameter-adaptive VMD method based on grasshopper optimization algorithm to analyze vibration signals from rotating machinery," *Mechanical Systems and Signal Processing*, vol. 108, pp. 58–72, 2018.

[18] D. Wang, Y. Zhao, C. Yi, K.-L. Tsui, and J. Lin, "Sparsity guided empirical wavelet transform for fault diagnosis of rolling element bearings," *Mechanical Systems and Signal Processing*, vol. 101, pp. 292–308, 2018.

[19] Z. Luo, T. Liu, S. Yan, and M. Qian, "Revised empirical wavelet transform based on auto-regressive power spectrum and its application to the mode decomposition of deployable structure," *Journal of Sound Vibration*, vol. 431, pp. 70–87, 2018.

[20] J. Antoni, "Fast computation of the kurtogram for the detection of transient faults," *Mechanical Systems and Signal Processing*, vol. 21, no. 1, pp. 108–124, 2007.

[21] S. Li, N. Chu, and P. Yan, "Cyclostationary approach to detect flow-induced effects on vibration signals from centrifugal pumps," *Mechanical Systems Signal Processing*, vol. 114, pp. 275–289, 2019.

[22] J. Li, J. Zhang, and M. Li, "A novel adaptive stochastic resonance method based on coupled bistable systems and its application in rolling bearing fault diagnosis," *Mechanical Systems Signal Processing*, vol. 114, pp. 128–145, 2019.

[23] H. Endo and R. B. Randall, "Enhancement of auto regressive model based gear tooth fault detection technique by the use of minimum entropy deconvolution filter," *Mechanical Systems Signal Processing*, vol. 21, no. 2, pp. 906–919, 2007.

[24] J. Li, M. Li, and J. Zhang, "Rolling bearing fault diagnosis based on time-delayed feedback monostable stochastic resonance and adaptive minimum entropy deconvolution," *Journal of Sound and Vibration*, vol. 401, pp. 139–151, 2017.

[25] D. Abboud, M. Elbadaoui, and W. A. Smith, "Advanced bearing diagnostics: A comparative study of two powerful approaches," *Mechanical Systems and Signal Processing*, vol. 114, pp. 604–627, 2019.

[26] G. L. McDonald, Q. Zhao, and M. J. Zuo, "Maximum correlated Kurtosis deconvolution and application on gear tooth chip fault detection," *Mechanical Systems and Signal Processing*, vol. 33, pp. 237–255, 2012.

[27] S. Wan, X. Zhang, and L. Dou, "Compound fault diagnosis of bearings using an improved spectral kurtosis by MCDK," *Mathematical Problems in Engineering*, vol. 2018, Article ID 6513045, 12 pages, 2018.

[28] G. L. McDonald and Q. Zhao, "Multipoint optimal minimum entropy deconvolution and convolution fix: Application to vibration fault detection," *Mechanical Systems and Signal Processing*, vol. 82, pp. 461–477, 2017.

[29] W. Cai, Z. Yang, Z. Wang, and Y. Wang, "A new compound fault feature extraction method based on multipoint kurtosis and variational mode decomposition," *Entropy*, vol. 20, no. 7, Article ID e20070521, 2018.

[30] Z. Wang, J. Wang, Z. Zhao, W. Wu, J. Zhang, and Y. Kou, "Composite fault feature extraction of gear box based on MKurt-MOMEDA," *Journal of Vibration, Measurement and Diagnosis*, vol. 37, no. 4, pp. 830–834, 2017 (Maltese).

[31] X. Zhu and Y. Wang, "Fault diagnosis of rolling bearings based on the MOMEDA and Teager energy operator," *Journal of Vibration Shock*, vol. 37, no. 6, pp. 104–110, 2018.

[32] Y. Wang, N. Hu, L. Hu, and Z. Cheng, "Rolling bearing fault diagnosis based on multipoint optimal minimum entropy deconvolution adjusted technique and direct spectral analysis," in *Proceedings of the 8th IEEE Prognostics and System Health Management Conference, PHM-Harbin 2017*, China, July 2017.

[33] Z. Wang, J. Wang, Z. Zhao, and R. Wang, "A novel method for multi-fault feature extraction of a gearbox under strong background noise," *Entropy*, vol. 20, no. 1, Article ID e20010010, 2018.

[34] W. Cai and Z. Wang, "Application of an improved multipoint optimal minimum entropy deconvolution adjusted for gearbox composite fault diagnosis," *Sensors*, vol. 18, no. 9, Article ID s18092861, 2018.

[35] Y. Cheng, N. Zhou, and W. Zhang, "Application of an improved minimum entropy deconvolution method for railway rolling element bearing fault diagnosis," *Journal of Sound Vibration*, vol. 425, pp. 53–69, 2018.

[36] J. Li, J. Jiang, X. Fan et al., "A new method for weak fault feature extraction based on improved MED," *Shock and Vibration*, vol. 2018, Article ID 9432394, 11 pages, 2018.

[37] Y. Miao, M. Zhao, J. Lin, and Y. Lei, "Application of an improved maximum correlated kurtosis deconvolution method for fault diagnosis of rolling element bearings," *Mechanical Systems and Signal Processing*, vol. 92, pp. 173–195, 2017.

[38] S. Saremi, S. Mirjalili, and A. Lewis, "Grasshopper optimisation algorithm: theory and application," *Advances in Engineering Software*, vol. 105, pp. 30–47, 2017.

[39] M. Barman, N. B. Dev Choudhury, and S. Sutradhar, "A regional hybrid GOA-SVM model based on similar day approach for short-term load forecasting in Assam, India," *Energy*, vol. 145, pp. 710–720, 2018.

[40] K. Loparo, *Bearings Vibration Data Set*, Case Western Reserve University, 2003, http://csegroups.case.edu/bearingdatacenter/pages/download-data-file.

[41] J. Lee, H. Qiu, and G. Yu, Rexnord technical services. Ims. University of cincinnati. "Bearing data set", NASA Ames prognostics data repository. Moffett Field, CA: NASA Ames Research Center; 2007. http://ti.arc.nasa.gov/project/prognostic-data-repository.

[42] S. Mirjalili, S. M. Mirjalili, and A. Lewis, "Grey wolf optimizer," *Advances in Engineering Software*, vol. 69, pp. 46–61, 2014.

[43] H. Sun, C. Wu, X. Liang, and Q. Zeng, "Identification of multiple faults in gearbox based on multipoint optional minimum entropy deconvolution adjusted and permutation entropy," *Entropy*, vol. 20, no. 11, Article ID e20110850, 2018.

[44] J. Ma, J. Wu, and X. Wang, "Incipient fault feature extraction of rolling bearings based on the MVMD and Teager energy operator," *ISA Transactions*, vol. 80, pp. 297–311, 2018.

[45] Y. Song, S. Zeng, J. Ma, and J. Guo, "A fault diagnosis method for roller bearing based on empirical wavelet transform decomposition with adaptive empirical mode segmentation," *Measurement*, vol. 117, pp. 266–276, 2018.

[46] K. Kumar, S. Shukla, and S. K. Singh, "A combined approach for weak fault signature extraction of rolling element bearing using Hilbert envelop and zero frequency resonator," *Journal of Sound and Vibration*, vol. 419, pp. 436–451, 2018.

[47] L. Duan, F. Zhao, J. Wang, N. Wang, and J. Zhang, "An integrated cumulative transformation and feature fusion approach for bearing degradation prognostics," *Shock and Vibration*, vol. 2018, Article ID 9067184, 15 pages, 2018.

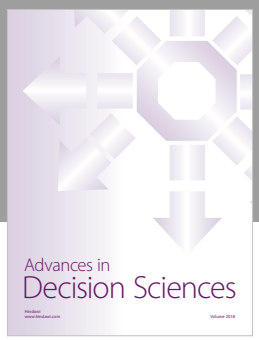

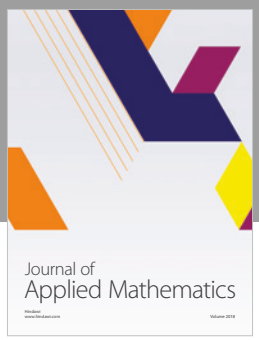

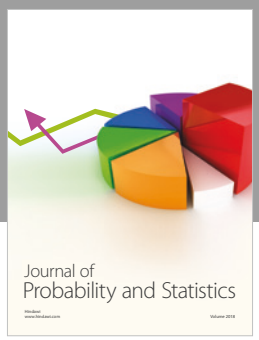

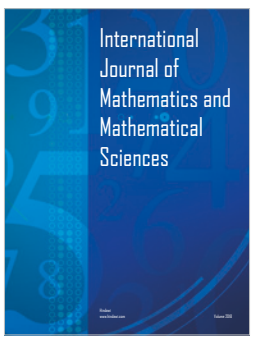

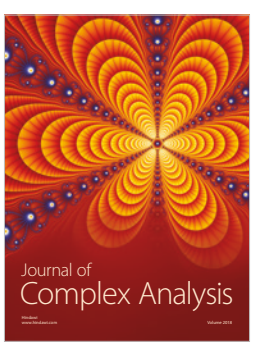

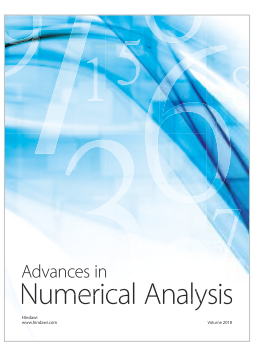

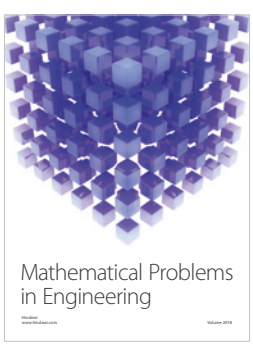

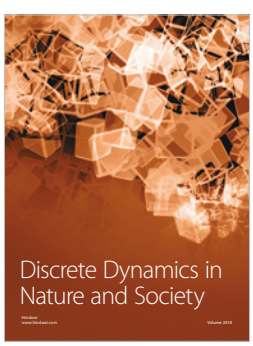

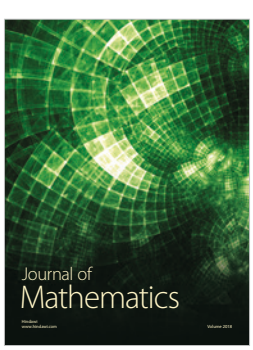

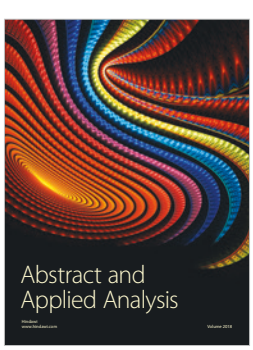

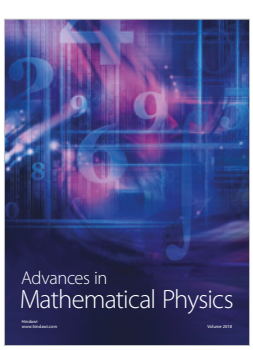

Hindawi

Submit your manuscripts at
www.hindawi.com